Most bivalves and gastropods calcify indistinguishably from dual clumped isotope equilibrium

Vanessa Schlidt[1]*, David Evans[1,2], Niels J. de Winter[3], Miguel Bernecker[1], Iris Arndt[1], Philip T. Staudigel[1], Amelia J. Davies[1,4], Uwe Brand[5], Wolfgang Müller[1], Jens Fiebig[1]

[1]Institute of Geosciences, Goethe University Frankfurt, Altenhöferallee 1, 60438 Frankfurt am Main, Germany

[2]Now at: School of Ocean and Earth Science, University of Southampton, Southampton, UK

[3]Department of Earth Sciences, Vrije Universiteit Amsterdam, the Netherlands

[4]Now at: Institute for Geology and Mineralogy, University of Cologne, Cologne, Germany

[5]Department of Earth Sciences, Brock University, St. Catharines, Ontario, Canada

*corresponding author: e-mail: schlidt@em.uni-frankfurt.de

Co-Authors: D.Evans@soton.ac.uk, n.j.de.winter@vu.nl, bernecker@em.uni-frankfurt.de, arndt@em.uni-frankfurt.de, staudigel@em.uni-frankfurt.de, adavies@uni-koeln.de, ubrand@brocku.ca, w.muller@em.uni-frankfurt.de, Jens.Fiebig@em.uni-frankfurt.de

Most bivalves and gastropods calcify indistinguishably from dual clumped isotope equilibrium

Vanessa Schlidt[1*], David Evans[1,2], Niels J. de Winter[3], Miguel Bernecker[1], Iris Arndt[1], Philip T. Staudigel[1], Amelia J. Davies[1,4], Uwe Brand[5], Wolfgang Müller[1], Jens Fiebig[1*]

[1]Institute of Geosciences, Goethe University Frankfurt, Altenhöferallee 1, 60438 Frankfurt am Main, Germany
[2]Now at: School of Ocean and Earth Science, University of Southampton, Southampton, UK
[3]Department of Earth Sciences, Vrije Universiteit Amsterdam, the Netherlands
[4]Now at: Institute for Geology and Mineralogy, University of Cologne, Cologne, Germany
[5]Department of Earth Sciences, Brock University, St. Catharines, Ontario, Canada

*corresponding authors: e-mail: schlidt@em.uni-frankfurt.de; Jens.Fiebig@em.uni-frankfurt.de

Abstract

Molluscan shell-carbonates are extensively used to reconstruct paleo-temperatures at sub-annual resolution. The accurate application of two widely used temperature proxies, the shell carbonate oxygen isotope ($\delta^{18}O$) and carbonate clumped isotope (Δ_{47}) composition, is based on the assumption that kinetics in the DIC-H_2O-$CaCO_3$ system were either absent or invariant during shell formation and/or can be corrected for via empirical calibration.

Here, we analysed the dual clumped isotope composition, i.e., Δ_{47} and Δ_{48}, of a wide range of modern and Eocene molluscs (bivalves and gastropods) to investigate the potential importance of kinetics during molluscan biomineralisation. We show that Δ_{47} and Δ_{48} of most of our modern samples are indistinguishable from equilibrium. For these samples, Δ_{47}-derived temperatures conform to corresponding growth temperatures within their fully propagated 95% uncertainties of $\leq$ +/-2.3°C. Significant departures from equilibrium values are only obtained for two samples characterised by growth temperatures <10°C. Together, these results strongly imply that bivalve and gastropod shell carbonates represent key archives for accurate and highly precise reconstructions of sea surface temperatures by means of Δ_{47} clumped isotope thermometry. Kinetic limitations of this thermometer may only become important at relatively low

temperatures. Δ_{47}-derived temperatures for our Eocene samples (~39 Ma) from the Hampshire Basin (paleo-latitude ~40°N)) show a range of 17.3-23.2°C. These paleo-temperatures are in good agreement with previous sea surface temperatures for the mid-Eocene mid latitude regions based on foraminifera clumped isotopes, adding confidence to both datasets.

In addition, in order to aid the accurate reconstruction of seawater $\delta^{18}O$ values, we compiled published oxygen isotope fractionation data for molluscs and established relationships that describe the temperature dependence of oxygen isotope fractionation between water and molluscan calcite and aragonite, respectively. Applying the equation for aragonite to the Eocene samples, we obtain reconstructed seawater $\delta^{18}O$ for the Hampshire Basin between -2.3‰ and -3.5‰ VSMOW

1. Introduction

Accurate reconstruction of Earth's surface temperatures during periods of elevated atmospheric CO_2 levels is of great importance for testing the robustness of climate models that are used to predict future climate change. To accomplish this task, it is necessary to identify geochemical proxies and sedimentary archives that reliably record Earth's surface temperatures in deep time, given that the most recent time interval characterised by a global climate state similar to the worst-case end-of-century CO_2 predictions occurred millions of years ago (e.g., Judd et al., 2024).

Molluscan shells represent a potential archive, that would allow for accurate climate reconstruction across such an extent of geological time. Molluscs make up one of the most diverse groups of calcifying organisms on Earth and cover a wide range of both terrestrial and marine habitats, while their (continuous) occurrence in the fossil record reaches back as far as the early Cambrian (e.g., Immenhauser et al., 2016 and references therein). They achieved dominance in abundance over brachiopods by the end of the Permian (Payne et al., 2014).

Molluscs form shells of calcite, aragonite, and sometimes high-Mg calcite and vaterite (Nehrke et al., 2012), and often combinations thereof. Mollusc-based paleo-temperature reconstructions have predominantly utilised the oxygen isotope composition ($\delta^{18}O$) of their shells (e.g., Schöne et al., 2005; Butler et al., 2015; Huyghe et al., 2015; de Winter et al., 2020, Ivany et al., 2022; Arndt et al., 2024), requiring the oxygen isotope composition of seawater to be known or assumed.

The carbonate clumped isotope thermometer (Ghosh et al., 2006) avoids this issue as it is based on the temperature dependence of the Δ_{47} value. This value compares the abundance of ^{13}C-^{18}O-bearing isotopologues in the CO_2 derived from phosphoric acid digestion of carbonates with its stochastically predicted abundance (Ghosh et al., 2006), which is independent of the oxygen isotope composition of seawater. Nonetheless, the attainment of homogeneous isotopic equilibrium in the solution from which $CaCO_3$ is precipitated (i.e., the isotopic equilibration between water and the DIC species) is a requirement for accurate temperature reconstructions using the Δ_{47}-thermometer. However, recent studies revealed that many carbonates which are precipitated biogenically (e.g., by corals, brachiopods, echinoids, and cephalopods) or inorganically (e.g., speleothems) record Δ_{47} signatures that are affected by rate-limiting kinetics (Affek, et al., 2014; Affek & Zaarur, 2014; Bajnai et al., 2018, 2020; Daeron et al., 2011; Davies & John, 2019; Davies et al., 2021; Guo, 2020; Guo & Zhou, 2019; Saenger et al., 2012; Saenger et al., 2017).

The rate-limiting step/reaction in the equilibration of both clumped and oxygen isotopes within the DIC-H_2O-$CaCO_3$ system is the interconversion of aqueous CO_2 and HCO_3^- via (de)hydration and (de)hydroxylation. If a carbonate's precipitation rate outpaces the equilibration rate of the DIC pool, the disequilibrium isotopic signatures present in the DIC pool will be inherited by the forming carbonate. The direction and magnitude of these kinetic biases is governed by processes, such as addition or removal of CO_2, that can perturb the state of DIC during mineral formation (Guo, 2020). Since both the oxygen and clumped isotope

composition of a carbonate follow the same chemical exchange reactions, $\delta^{18}O_{carb}$ and Δ_{47} can be used in conjunction to detect potential kinetic biases (e.g., Bajnai et al., 2018). Still, the uncertainties introduced by unknown paleo-water $\delta^{18}O$ values impair applications of paired $\delta^{18}O_{carb}$ and Δ_{47} measurements for diagnosis of kinetic biases in fossil archives. The presence of kinetic biases in the determination of carbonate formation temperatures through oxygen isotope and Δ_{47} thermometry can be overcome applying species-specific temperature calibrations (e.g., Weber & Woodhead, 1972; McConnaughey et al., 1989a; Davies et al., 2023) provided disequilibrium offsets are invariant through space and time.

The addition of a second thermodynamically controlled metric that is independent of fluid-$\delta^{18}O$ has become possible through high-precision Δ_{48} analysis, which addresses measured and stochastic abundances of m/z 48 isotopologues (mainly $^{12}C^{18}O_2$) in the CO_2 evolved from phosphoric acid digestion of carbonates (Fiebig et al., 2019). Δ_{47} and Δ_{48} and their precursor value in the carbonate, Δ_{63} and Δ_{64}, respectively, are controlled by the same chemical processes. Their simultaneous measurement, i.e., dual clumped isotope analysis, allows for the identification of disequilibrium dual clumped isotope signatures, the assessment of the extent of disequilibrium and the identification of the underlying process through which carbonate precipitation was initiated, by comparing measured dual clumped isotope data with the position of Δ_{47}-Δ_{48}-equilibrium (e.g., Bajnai et al., 2020; Fiebig et al., 2021). For example, if supersaturation and precipitation is achieved by CO_2 absorption, as is the case in corals (e.g., Thiagarajan et al., 2011; Saenger et al., 2012; Spooner et al., 2016) kinetic limitation will be expressed in $+\Delta_{47}$ and $-\Delta_{48}$ offsets from equilibrium (Guo, 2020; Bajnai et al., 2020). If, on the contrary, supersaturation and precipitation goes along with net CO_2 degassing, as is characteristic for speleothems, kinetic limitation evokes $-\Delta_{47}/+\Delta_{48}$ disequilibrium patterns (Guo & Zhou, 2019; Guo, 2020; Bajnai et al., 2020). Since its invention, dual clumped isotope thermometry has been used to identify kinetic bias in cold and warm water corals (Davies et al., 2022), brachiopods (Davies et al., 2023), bird eggshells (Tagliavento et al., 2023),

speleothems (Bajnai et al., 2020, Parvez et al., 2024), authigenic methane seep carbonates (Staudigel et al., 2024), freshwater cements (Lu et al., 2024), microbe-associated dolomites (Lu & Swart, 2024), and in carbonates associated with the serpentinization of ultramafic rocks (Parvez et al., 2023). Crucially, it has been shown that kinetic biases in corals, brachiopods, speleothems and methane seep carbonates follow identifiable, model predicted disequilibrium trajectories. These can be used to correct measured dual clumped isotope data and, finally, to isolate the temperature signal recorded in the carbonate. If, on the contrary, these kinetic biases remain undetected, as would be the case without having Δ_{48} accessible, these would lead to over- or underestimation of Δ_{47}-derived temperatures in case CO_2 absorption or CO_2 degassing were rate-limiting.

Previous investigations revealed that kinetic biases in Δ_{47} values of mollusc shells, if present at all, might only be weakly pronounced. Huyghe et al. (2022) and de Winter et al. (2022) analysed shells of marine bivalves and oysters grown at temperatures of -2 to 27°C. With the exception of juvenile oysters, Δ_{47} values obtained by Huyghe et al. (2022) agreed with those predicted by the unified calibration of Anderson et al. (2021) which, in turn, is indistinguishable from the inorganic calcite equilibrium Δ_{47}-T relationship of Fiebig et al. (2021). On the contrary, formation temperatures for *A. islandica* were slightly, but significantly (2.7 ± 2.0°C) underestimated by de Winter et al. (2022) who also projected Δ_{47} values to Anderson et al. (2021). Curley et al. (2023) investigated fossil bivalve mollusc shells of unconstrained growth temperatures. Based on intra-shell alignments between Δ_{47} and $\delta^{18}O_{carb}$ they postulated that the inner shell layer is prone to kinetic isotope effects, whereas the outer shell layer is not.

In this study, we analysed the dual clumped isotope composition of twelve modern and five fossil mollusc species for an overall total of 21 specimen to investigate whether their clumped isotope composition is affected by rate-limiting kinetics. We demonstrate that significant kinetic departures from equilibrium only seem to occur at low temperature (< 10°C) which makes bivalves and gastropods ideal archives for high-precision paleo-temperature

reconstructions for moderate to warm climates using Δ_{47} thermometry. Our assessment that kinetic biases may become important at low temperature is in agreement with the observation that compiled mollusc-specific $1000\ln\alpha(CaCO_3\text{-}H_2O)$ for aragonite and calcite increasingly deviate from equilibrium $\alpha(\text{Calcite-}H_2O)$ (Coplen, 2007) towards lower values with decreasing temperature. Finally, we apply the dual clumped isotope thermometer to five Eocene samples from the Hampshire Basin, reconstruct temperatures and seawater $\delta^{18}O$, and compare these estimates to data previously reconstructed for the same geographic region and age.

2. Material and Methods

In this study, we analysed twenty-one molluscan samples for their dual clumped and stable isotope compositions, i.e., sixteen modern specimens and five shells from the mid Eocene (Bartonian; ~39 Myr). Metadata for all samples is given in Table 1.

2.1 Modern samples

Sample names and details of modern samples measured in this study are given in Table 1. The bivalves *M. modiolus* (RM1) and *S. solida* (RM2) as well as the gastropods *B. undatum* (RG1) and *P. vulgata* (RG2) were collected at low tide from a beach in southeast Scotland (Tentsmuir Forest) in March 2020. The average annual sea surface temperature for the site of sample collection is 9.7°C determined using the World Ocean Atlas 2013 (WOA 2013; Locarnini et al., 2013), with a seasonal range of 6-14°C. The oxygen isotope composition of seawater at the site of sample collection was calculated based on grid data provided by Harwood et al. (2008) ($\delta^{18}O_{sw}$ (VSMOW) = 0.2‰).

Some material for this study came from a population of cultured bivalves: *A. islandica* (AI_006) and *M. edulis* (ME_002, ME_003) grew in culture at NIOZ (Royal Netherlands Institute for Sea Research). Growth temperatures for ME_002 and ME_003 range between 5-25°C (seasonal temperature changes were imposed on these cultures) with an average growing season temperature of 16.2°C during the culturing period. AI_006 was cultured at 12°C.

M2-Sf and M2-Sv are sample powders from a cultured *M. gigas* (also known as *C. gigas*) specimen (additional geochemical data published in de Winter et al., 2021a). The seasonal range of temperatures for M2-Sf and M2-Sv varies between 4-19°C with a mean annual SST of 11.5°C. Reconstructed $\delta^{18}O_{sw}$ (VSMOW) is -1.55‰ (de Winter et al., 2021a). CHA_M_050 and CHA_M_062 represent *A. islandica* specimen which were collected off the coast of NE Iceland (Pederson et al., 2019). Their estimated mean growth temperature is 3-4°C, although summer temperatures may exceed 10°C. Dual clumped isotope data has already been reported and discussed by Staudigel et al. (2023a). Bivalves Shell UC and Shell UH, both of the species *H. porcellanus*, were purchased at an antique trade; growth temperature and $\delta^{18}O$ values of the water are therefore unknown, although growth temperatures can be approximately estimated because *H. porcellanus* has a narrow distribution in the modern ocean. This species mainly occurs in Indonesia, Palau, and the Philippines for which the WOA2013 lists mean annual SST's of 27-31°C (Levitus et al., 2015). *H. arctica* (WS2) and *T. borealis* (WS3) originate from the White Sea (Barents Sea) which exhibits a mean annual SST of 5.6°C (seasonal range <0-10°C) (WOA2013). A $\delta^{18}O_{sw}$ (VSMOW) of -3.83‰ was measured in situ. Bivalve *T. squamosa* (TS2) grew in a large zoo aquarium with an average water temperature of 25.9°C and $\delta^{18}O_{sw}$ (VSMOW) of -1.05‰ (Batenburg et al., 2011).

2.2 Eocene samples

The Eocene samples were collected from the Barton Clay Formation (base of the Naish member) at Barton-on-Sea (southern UK). The analysed species are the gastropods *Sycostoma* sp. COX 1931 (FG1), *Orthosurcula rostrata* (SOLANDER 1766) (FG2), *Strombus athleta* (SOLANDER 1766) (FG3) and bivalves *Bathytormus sulcata* (SOLANDER 1766) (FM1) and *Arcturellina pusilla* (DESHAYES 1858) (FM2). They were collected from the same area as sample SW1 analysed by Evans et al. (2018) from the Hampshire Basin, but are of a slightly younger age (39.5-40.5Ma) than SW1.

All Eocene mollusc shells are fully preserved and consist of 100% aragonite determined by Powder X-Ray diffraction (XRD)

2.3 Sample preparation

In the case of RM1, RM2, RG1, and RG2 the entire shell was crushed to sub-cm sized fragments and then ground to powder using an agate mortar and pestle. For samples WS2 and WS3 material was taken avoiding the muscle scars, ventral margin and palial sinus, umbo and hinge. These shells were cleaned by buffing the outer layer with a dremel. Samples Shell UC and Shell UH were removed as circular cores from individual growth bands using a drill, and were subsequently homogenised with a mortar and pestle. Shell UH was analysed for fluid inclusion $\delta^{18}O$ prior to being homogenised as described in Nooitgedacht et al. (2021). In the case of TS2, a section was cut out of the inner shell and ground to a fine powder using an agate mortar and pestle.

The sample preparation for M2-Sf and M2-Sv is described in de Winter et al. (2021a). M2-Sf samples a sufficiently large portion of the shell to represent the mean annual temperature at which the specimen grew. M2-Sv is a sample that averages shell material formed throughout the second growth year of the specimen.

In the case of ME_002, ME_003, and AI_006 the bulk shell parts that were grown in culture were sampled (i.e., no differentiated sampling of the outer and inner shell). Samples CHA_M_050 and CHA_M_062 consist of bulk powder homogenised from *A. islandica* collected from NE Iceland in 2010 (Staudigel et al., 2023a; Pederson et al., 2019).

The Eocene samples FG1, FG2, FG3, FM1, and FM2 were crushed to smaller pieces using a hammer. These pieces were cleaned by scraping clay residues off with a spatula and rinsing the shell fragments with deionised (DI) water in an ultrasonic bath. They were ground to powder with an agate mortar and pestle.

With the exception of samples RM1, RM2, RG1, and RG2, which were subjected to oxidative cleaning using a ~3 wt-% NaOCl solution (Fiebig et al., 2024), the powders did not undergo

any pre-treatment for organic matter removal. After reacting overnight, the NaOCl solution was discarded and the powders rinsed with DI water before being left to dry at room temperature for several days. All sample powders were stored in a vacuum dryer at 30°C before the analyses. Non-bleached aliquots (n = 6) of RG2 were analysed along with bleached (n = 9) aliquots. We did not detect any significant differences in the dual clumped isotope compositions for the two sets of sub-samples (see Supplementary Figure S1). Thus, we conclude that interfering components that release NO_2 (Fiebig et al., 2024) were absent, and that oxidative cleaning did not affect the dual clumped isotope compositions of our sample powders. As such, both sub-sets of RG2 aliquots were pooled for the purpose of data interpretation.

2.4 Mass spectrometric analyses and data processing

All samples were analysed for their Δ_{47}, Δ_{48}, $\delta^{18}O$ and $\delta^{13}C$ values following the experimental setup of Fiebig et al. (2019) and methodology described by Bernecker et al. (2023). For the dual clumped isotope measurements, 10 mg (±0.2 mg) per replicate were weighed into silver capsules; 6-15 replicates were analysed for each sample. Acid digestion took place in a common acid bath at 90°C using phosphoric acid (>108 wt-%). ETH-1, ETH-2, non-bleached ETH-3, in-house Carrara marble as well as CO_2 gases equilibrated at 25°C and 1000°C, respectively, were analysed alongside the samples. The preparation process of equilibrated and heated gases followed the procedure described in Bernecker et al. (2023). All samples, standards, and gases were measured against a reference gas with the following isotopic compositions: $\delta^{13}C_{VPDB}$ = -4.2‰ and $\delta^{18}O_{VSMOW}$ = 25.26‰ (ISO-TOP, Air Liquide, France).

Dual clumped data processing followed the method described in Bernecker et al. (2023), using optimal scaling factors for pressure baseline correction based on continuously monitored m/z 47.5 intensities and slope minimization algorithm for δ^{47} vs. Δ_{47} and δ^{48} vs. Δ_{48} correlations of equilibrated gas data. Background corrected raw data was normalised to the Carbon Dioxide Equilibrium Scale for an acid digestion temperature of 90°C (CDES 90) (Dennis et al., 2011)

using D47crunch (Daëron, 2021), pooling over all sessions and considering equilibrated gases as anchors exclusively. For this purpose, non-bleached replicates of ETH-3 were labelled individually in order to avoid any bias introduced by the variance algorithm of D47crunch (Fiebig et al., 2024). Reported uncertainties represent fully propagated 2 SE, considering allogenic and autogenic errors.

$\delta^{18}O$ values of carbonate samples analysed in this study were normalized against nominal values of ETH-1 and ETH-2 (Bernasconi et al., 2018). Since these ETH standards represent calcite, $\delta^{18}O$ values obtained for aragonite were corrected for the difference in acid fractionation factors between calcite and aragonite at 90°C (Kim et al., 2007b). For samples of mixed mineralogy (*P. vulgata*, *M. edulis*), we applied the acid fractionation factors for both, calcite and aragonite, (Kim et al., 2007b) according to their percentile abundance in the sample.

2.5 Re-evaluating the temperature dependence of the oxygen isotope fractionation between mollusc carbonate and water

In order to re-evaluate the temperature dependence of the oxygen isotope fractionation between mollusc shell-carbonate and seawater, we compiled $\delta^{18}O$ data on aragonite, calcite, and seawater from Grossman and Ku (1986), Lecuyer et al., (2004, 2012), Henkes et al. (2013), Caldarescu et al. (2021), Huyghe et al. (2022), and de Winter et al. (2022). Further, we considered data on our investigated modern specimens (Tables, 1, 2). Compiled data sets are available in Supplementary Table S1. Specimen-specific oxygen isotope data was considered in all cases. De Winter et al. (2022) originally provided high-resolution data on four specimens, so we calculated specimen-specific mean $\delta^{18}O$ values from their data in order to avoid over-representation. The aragonitic samples of Grossmann and Ku (1986) were originally acid digested at 50-60°C and calibrated against NBS 19 calcite. In order to account for the difference in acid fractionation factors between aragonite and calcite, we, therefore, considered the equation for acid fractionation for calcite by Kim et al. (2007b) (T = 55°C) to calculate $\delta^{18}O_{CO2}$

from the given $\delta^{18}O_{\text{"shell"}}$ and then their equation for aragonite (T = 55°C) to obtain $\delta^{18}O_{aragonite}$. Oxygen isotope fractionation factors for aragonite and calcite were calculated from published oxygen isotope compositions according to (1)

$$\alpha_{carb\text{-}H2O} = \frac{\delta^{18}O_{cc}+1000}{\delta^{18}O_{H_2O}+1000} \quad (1)$$

Uncertainties for oxygen isotope input data are not consistently reported in the studies of Grossman and Ku (1986), Lecuyer et al., (2004, 2012), Henkes et al. (2013), Caldarescu et al. (2021), Huyghe et al. (2022) and de Winter et al. (2022). An error-weighted linear regression would, therefore, add more weight to data that lacks any reported uncertainties, which needs to be avoided. Consequently, we did not consider these uncertainties in compiled $\alpha_{carb\text{-}H2O}$ values and growth temperatures.

3. Results

Table 2 lists the stable and clumped isotope compositions of all samples analysed in this study as well as their respective uncertainties. Baseline-corrected input data (δ^{45}-δ^{49}) as well as Δ_{47}, Δ_{48}, $\delta^{18}O$, and $\delta^{13}C$ results, along with processing statistics, can be found in Supplementary Tables S2 and S3. Dual clumped isotope data of the modern molluscs is compared to the position of equilibrium (Fiebig et al., 2021, revised after Fiebig et al., 2024) in Figure 1. With the exception of two specimens (RG2, WS3), all modern molluscs plot indistinguishably from equilibrium. The Δ_{47}-derived temperatures and corresponding seasonal ranges of growth temperatures are displayed in Table 3. The dual clumped isotope compositions of the Eocene samples are displayed in Figure 2 relative to dual clumped equilibrium (Fiebig et al., 2024). All fossil specimens exhibit dual clumped isotope compositions that are indistinguishable from equilibrium within their uncertainties.

$1000\ln\alpha(CaCO_3\text{-}H_2O)$-1/T relationships for calcite and aragonite are displayed in Figure 3a and 3b, respectively, yielding the following Equations 2 and 3:

Aragonite: $1000\ln(\alpha) = 16.435\ (\pm 0.424) \times (10^3/T) - 25.61\ (\pm 1.46)$, (2)

$R^2 = 0.90$, n = 154

Calcite: $1000\ln(\alpha) = 15.665\ (\pm 0.832) \times (10^3/T) - 23.63\ (\pm 2.87)$, (3)

$R^2 = 0.81$, n = 81

In order to constrain the sensitivity of the regressions to possible outliers in the two data sets, we compare the above ordinary least-squares regression to those resulting from a bootstrapping approach, in which the individual data sets were randomly resampled 10000 times, adding higher weight to random individual samples by resampling with replacement. Each outcome was fit using ordinary least-squares regression again. The overall results, based on the 50^{th} percentile of the 10^4 regression coefficients, are shown in Supplementary Figure S2. These demonstrate that the difference between the original and resampled approach results in calibrations that differ by less than 0.12‰ across the entire investigated temperature range.

Figure 3c compares these relationships intervals with the corresponding calibration regression lines for inorganic calcite after Kim & O'Neil (1997) and Coplen (2007), and for inorganic aragonite after Kim et al. (2007a).

4. Discussion

4.1 Dual clumped isotope thermometry on modern mollusc shells

Although most modern samples have dual clumped isotope compositions that fall within uncertainty of equilibrium, this observation, on its own, does not provide hard evidence that equilibrium has been attained in each of these cases. A comparison of measured growth temperatures with Δ_{47}-derived growth temperatures is necessary to prove this hypothesis in more detail. This comparison allows us to identify samples that could have been affected by two or more rate-limiting kinetic processes which – in combination - lead to Δ_{47} and Δ_{48} values plotting fortuitously indistinguishable from equilibrium, as was observed for individual brachiopods (Davies et al., 2023). Δ_{47}-derived temperatures for samples *B. undatum* (RG1), *M. modiolus* (RM1) and *S. solida* (RM2), which are apparently in equilibrium (Fig. 1), are 6.9°C

(±2.2°C, 95CI), 8.2°C (±2.3°C, 95CI) and 8.2°C (±2.3°C, 95CI), respectively. These values agree with the mean annual sea surface temperature (MASST) of 9.7°C and/or the seasonally monitored temperature range of 6-14°C reported for the beach at Tentsmuir Forest within their errors (Table 3). A fourth sample, *P. vulgata* (RG2) was collected at the same sample location. Its Δ_{47}-derived temperature of 9.1°C (±1.6°C, 95CI) is consistent with the MASST of 9.7°C (Table 3); however, its Δ_{48}-value exhibits a slightly positive, but significant bias relative to the equilibrium Δ_{48}-value expected for this temperature. Fiebig et al. (2024) found that a NO_2 interference can cause $-\Delta_{47}/+\Delta_{48}$ offsets from equilibrium. However, NO_2 interference can be excluded in this case since the mean Δ_{47} and Δ_{48} values of bleached and unbleached aliquots of that sample were indistinguishable from each other (Supplementary Figure S1). The outer and inner shell areas of RG2 consist of calcite and aragonite, respectively; such that our powder sample is of mixed mineralogy. The $\delta^{18}O$ values of both phases, however, differ by less than 1‰ such that non-linear mixing also cannot explain the observed offset from equilibrium (Staudigel et al., 2023a,b; White & Defliese, 2023). Since artificial biases like mixing and NO_2 interference can be excluded, the observed disequilibrium signature of RG2 may, therefore, be of a kinetic nature.

Δ_{47}-derived temperatures for all three specimens of *A. islandica* (AI_006, CHA_M_050, and CHA_M_062), all of which plot indistinguishable from equilibrium (Fig. 1), confirm independently known growth temperature ranges (Table 3). For AI_006, which was grown in culture at a constant temperature of 12.0°C, we reconstruct a temperature of 12.3°C (±2.3°C). CHA_M_050 and CHA_M_062 were collected from the NE Iceland margin alongside molluscs analysed in Pederson et al. (2019). Δ_{47}-derived temperatures for these samples are 7.6°C (±2.3°C) and 5.1°C (±2.3°C), respectively. Mean water temperatures of 3-4°C were estimated for the site of sample collection but may exceed 10°C depending on the season. We therefore conclude that the most likely explanation for this offset towards warmer temperature reconstructions may be due to preferential shell growth during summer months, as has been

observed for some molluscs (e.g., Vitahkari et al., 2016; Witbaard et al., 1994; Goodwin et al., 2001; Kaandorp et al., 2003; Judd et al., 2017; de Winter et al., 2021a,b).

The sampled parts of the mussels *M. edulis* ME_002 and ME_003 grew in culture, at 5-25°C with a mean temperature of 16.2°C, although temperature was briefly raised/lowered to 31°C and 3°C, respectively, over a short period of time for the purpose of conducting respiration rate experiments (Jansen et al., 2007). Δ_{47}-derived temperatures for ME_002 and ME_003 are 16.1°C (±2.2°C) and 15.4°C (±2.3°C), respectively (Table 3), aligning well with estimated mean growth temperatures and therefore, confirming that dual clumped isotope equilibrium has been attained (Fig. 1).

Samples of the oyster *M. gigas* (M2-Sf and M2-Sv) also plot indistinguishably from the equilibrium line within uncertainty (Fig. 1). These samples were taken from the same oyster shell. Measured Δ_{47}-values correspond to temperatures of 19.0°C (±2.1°C) and 12.1°C (±1.9°), respectively (Table 3). The sample powders originate from two different small areas of the shell with different microstructure, i.e., from the foliated calcite in the hinge (M2-Sf) and from the chalky calcite material of the second growth year (M2-Sv) (see de Winter et al., 2021a,b for more information). Both sample powders represent averages of material grown across seasons, with their Δ_{47}-derived temperatures therefore potentially representing either mean annual or seasonal temperature, depending on when growth occurred (seasonal range of growth temperatures = 4.5-19.2°C, mean = 11.5°C, Table 3). M2-Sf exhibits a Δ_{47} temperature that corresponds to the maximum seasonal temperature. The colder Δ_{47} derived temperature formation temperature of 12.1°C (±1.9°) for M2-Sv, on the contrary, is in excellent agreement with the measured mean annual temperature of 11.5°C. The different temperatures obtained for M2-Sf and M2-Sv might stem from sampling bias. Given that the two samples are from the same species a different calcification response to temperature change would not be expected. Instead, considering that only small areas were sampled, it is more likely that the powders represent different seasonal stages of growth.

Three *Tridacninae* from both the natural environment and an aquarium, including two different species, were analysed. The exact locations at which *H. porcellanus* (Shell UC and Shell UH) were collected are unknown. However, based on the limited geographic range of Indonesia, the Philippines and Palau, an average water temperature of about 27-31°C can be taken as a gross approximation (Levitus et al., 2015). Both samples plot indistinguishably from apparent equilibrium (Fig. 1) and yield Δ_{47}-derived growth temperatures of 26.3°C (±2.3°C, 95% CI) and 28.3°C (±2.2°C, 95CI), respectively (Table 3). *T. squamosa* (TS2), which also plots within errors indistinguishably from the equilibrium line (Fig. 1), was cultured in an aquarium kept at near-constant temperature. The Δ_{47}-derived temperature of 24.4°C (±2.2°C, 95CI) agrees with the mean growth temperature of 25.9°C (up to 26.8°C during summer) (Batenburg et al., 2011; Janse et al., 2008) within uncertainty (Table 3).

Samples *H. arctica* (WS2) and *T. borealis* (WS3) from the White Sea show variable disequilibrium effects. WS2 plots significantly above the equilibrium line (Fig. 1) and is characterised by a Δ_{47}-derived temperature of 1.4°C (±1.8°C, 95CI) which is significantly colder than the MASST of 5.6°C (Table 3). The dual clumped isotope composition of WS3, on the contrary, plots within errors on the equilibrium line. Its Δ_{47}-derived temperature is 8.3°C (±2.0°C) which is slightly warmer than the estimated MASST, although still within the range of seasonal sea surface temperatures characteristic of the White Sea (-1.7°C to 10°C) (Table 3). This discrepancy between the observed and Δ_{47}-derived temperatures for samples WS2 and WS3 are discussed in detail in Section 4.3.

Overall, most specimens that have dual clumped isotope compositions indistinguishable from equilibrium are characterised by Δ_{47}-derived temperatures that are in good agreement with observed (seasonal) growth temperatures. This strongly implies that the internal arrangement of isotopes during precipitation often proceeds up to equilibrium. Bulk mollusc shell samples may, therefore, provide a robust archive for accurate and highly precise temperature reconstructions by means of Δ_{47} thermometry. Potential seasonal biases due to preferential

386 growth during summer need to be considered, especially when analysing bulk shells from mid-
387 high latitude regions. In case carbonate shells are run for Δ_{47} exclusively, care should be taken
388 if Δ_{47} indicates temperatures <10°C. At such low temperatures, kinetics may become relevant
389 and Δ_{48} should be analysed along with Δ_{47} in order to identify potential kinetic bias.

390 **4.2 Key parameters affecting biomineralisation of molluscs**

391 Of all analysed shells, only two samples, *H. arctica* (WS2) and *P. vulgata* (RG2), are
392 characterized by disequilibrium dual clumped isotope signatures (Fig. 1). Both specimens have
393 in common that they grew at relatively low temperatures of <10°C. For *P. vulgata* we also note
394 that this species lives in the intertidal zone, which may contribute to the observed disequilibrium
395 (more detailed discussion see Section 4.3).
396 Our observation that most of the investigated bivalve mollusc shells represent close -to-
397 equilibrium calcifiers differs from what is known about other marine calcifying organisms. For
398 example, corals have been shown to exhibit disequilibrium dual clumped isotope compositions;
399 their departure from equilibrium has been proposed to be the result of CO_2 absorption during
400 coralline carbonate formation (Bajnai et al., 2020; Davies et al., 2022). Corals actively elevate
401 the pH at their site of calcification (SOC) above ambient seawater pH, due to addition of Ca^{2+}
402 or Na^+ into the calcifying fluid and charge-balance-removal of H^+ (e.g.; Spooner et al., 2016;
403 Venn et al., 2019). During this process, aqueous CO_2 from ambient seawater and/or the ambient
404 tissue cells diffuses into the SOC along its concentration gradient. At the SOC, this CO_2 is then
405 transformed into bicarbonate via CO_2 hydration/hydroxylation. These two reactions and their
406 reverse reactions, dehydration/dehydroxylation, are rate-limiting in the DIC-water system, and,
407 therefore, in the accompanying oxygen isotope exchange among the different DIC species and
408 water (McConnaughey, 1989b; Adkins et al., 2003; Sade and Halevy, 2017; Affek, 2013; Guo
409 2020). Protonation/deprotonation of carbonate/bicarbonate, on the contrary, occurs almost
410 instantaneously such that metastable chemical and isotopic equilibrium between both species
411 is obtained at any time (McConnaughey, 1989b; Adkins et al., 2003; Chen et al. 2018).

Achieving oxygen and clumped isotope equilibrium in the DIC-H_2O system thus depends on the relative rates of CO_2 hydration/hydroxylation, bicarbonate dehydration/dehydroxylation and precipitation. If precipitation proceeds faster than isotopic equilibration of the DIC pool, disequilibrium signatures will be recorded in the forming carbonate (e.g., McConnaughey, 1989b; Adkins et al., 2003; Chen et al. 2018; Guo, 2020; Bajnai et al., 2020). In the case of cold and warm water corals (Davies et al., 2022), the dehydration/dehydroxylation reactions are slowest such that the isotopic composition of the precipitated carbonate largely records the kinetic isotope effects associated with the hydration/hydroxylation reactions of CO_2, resulting in lighter-than-equilibrium $\delta^{18}O$, $\delta^{13}C$, and Δ_{48}, but heavier Δ_{47} (Guo, 2020).

In the case of molluscs, the extrapallial fluid (EPF), in which precipitation takes place, is enclosed by the calcifying cells of the mantle epithelium as well as the periostracum, an organic layer covering the shell and extending over its edge (Fig. 4). The intra-cellular pH of the mantle cells is known to be around 7.4-7.5, while the EPF is characterised by a pH of ~7.8 (Ip et al., 2006) but may get as low as 7.2 (Crenshaw, 1972). The cell plasma being slightly more acidic than the EPF will result in diffusion of (metabolic) CO_2 from the surrounding cells into the EPF. The rate of (de)hydration/(de)hydroxylation reactions, and thus the rate at which isotopic equilibration of the DIC-H_2O system is achieved, is largely affected by factors such as pH and temperature, with higher pH and lower temperatures resulting in slower isotopic equilibration rates (e.g., Guo, 2020). The rate-dependence of the attainment of equilibrium on pH might offer an explanation for why molluscan shell carbonates exhibit equilibrium dual clumped isotope compositions while skeletons of corals do not. Unlike corals which elevate the pH at the SOC above seawater pH to initiate calcification, molluscs lower the pH of the EPF (which in molluscs is the equivalent to the SOC in corals) by 0.5-0.6 units relative to ambient seawater (cf. Crenshaw, 1972). At 25°C, isotopic equilibration of the DIC-H_2O system at a pH of 7.7 is predicted to proceed five times faster than at a pH of 8.7 that likely prevails at the SOC of some corals (e.g., Ross et al., 2022 and references therein) (Guo, 2020). At 10°C and 5°C, on the

contrary, the overall equilibration rate at a pH of 7.7 is reduced by a factor of 3 and 5, respectively, relative to 25°C, consistent with our observation that kinetic isotope effects are only recorded in molluscs grown at relatively low temperatures. The absolute rate of equilibration furthermore depends on the absence/presence of the enzyme carbonic anhydrase (CA). CA catalyses the hydration of CO_2 (e.g., Freeman & Wilbur, 1948; Nielsen and Frieden, 1972; Uchikawa and Zeebe, 2012; Le Roy et al., 2016) using Zn^{2+} as central ion in order to polarise, and therefore activate, water for the reaction (Park & Lee, 2019). The presence of CA has been observed in both corals (e.g., Uchikawa and Zeebe, 2012; Bertucci et al., 2013) and molluscs (e.g., Freeman and Wilbur, 1948; Nielsen and Frieden, 1972). CA has been found to be directly involved in molluscan shell formation, e.g., in the matrix during nacre production (Marie et al., 2008), as domain in nacrein (a protein important for nacre-formation) (Miyamoto et al., 1996) as well as in the mantle cells (Cardoso et al., 2019). In molluscs, proteins like nacrein inhibit calcium carbonate crystallisation from supersaturated solutions (Miyamoto et al., 2005), possibly to enable the organisms to tightly control the rate of calcification. In addition to pH and temperature, the presence of CA and nacrein may, therefore, be essential for the attainment of equilibrium in the molluscan DIC-H_2O-$CaCO_3$-system.

4.3 Kinetic biases and the potential impact of sample habitat

The equilibrium offset of *H. arctica* (WS2) (Fig. 1) may be caused by the slow rate of dehydration/dehydroxylation reactions at the low growth temperature of this sample, such that metabolic CO_2 is unidirectionally reacted to bicarbonate, without sufficient time to isotopically re-equilibrate with dissolved CO_2. The same CO_2-absorption kinetics are known to introduce $+\Delta_{47}/-\Delta_{48}$ offsets from dual clumped isotope equilibrium in other biogenic carbonates such as corals and brachiopods (Davies et al., 2022; Davies et al., 2023). The extent of this disequilibrium $+\Delta_{47}/-\Delta_{48}$ bias has been shown to be governed not only by temperature and pH, but also by the $\delta^{13}C$ of metabolic CO_2, CA activity, and the time that remains for isotopic equilibration prior to the onset of precipitation (e.g., Guo et al., 2020; Davies et al., 2022; Davies

et al., 2023). Based on the analysis of a single specimen it is impossible to propose a correction procedure. *H. arctica* (WS2) and *T. borealis* (WS3) grew in the same location and thus, were exposed to the same temperatures, but do not show the same bias (Fig. 1). Species-specific differences in growth rates or activity of CA may explain why WS2 has a kinetic bias while the dual clumped isotope composition of WS3 corresponds to equilibrium.

A single measured sample of *P. vulgata* (RG2) plots below the equilibrium line in dual clumped isotope space (Fig. 1). Its Δ_{47} value, however, corresponds to MASST at its growth site (Table 3). *P. vulgata*, a common limpet occupying an intertidal habitat, is submerged at high tides and exposed to air at low tides. Gas exchange with the surrounding environment during times of emersion is restricted in order to prevent desiccation (e.g., Burnett, 1988). To counteract the resulting hypercapnia (i.e., the accumulation of metabolic CO_2 which leads to acidification of the haemolymph) parts of the (inner) shell are dissolved (Lindinger et al., 1984). During this process, the DIC concentration of the EPF thus increases. It has been postulated that CO_2-degassing might occur as soon as the mollusc is submerged again and gas exchange with the surrounding water resumes (Curley et al., 2023). It has also been postulated that calcification rates in intertidally living species are accelerated during times of submersion (Tagliarolo et al., 2013a,b) but cease during emersion. This acceleration of growth rate may be explicable by the fact that the organism is in contact with seawater, from which the ions for calcification are ultimately derived, for less time than subtidal species. In addition, amorphous calcium carbonate (ACC) has been observed in some species (Weiss et al., 2002; Nassif et al., 2005; Jacob et al., 2011), representing a transient precursor of more stable crystalline aragonite or calcite (see e.g., Addadi et al., 2003, 2006). Tagliavento et al. (2023) showed that high Mg-calcite formed via ACMC, exhibited a significant $+\Delta_{48}$ bias relative to the Δ_{48} calcite equilibrium value predicted by its formation temperature, whereas its Δ_{47} corresponded to that temperature. The disequilibrium $+\Delta_{48}$ bias of RG2 may, therefore, imply that ACC is involved in the biomineralization process of *P. vulgata*. If so, the absence of a such a bias in *M. edulis*

(samples ME_002 and ME_003), in which aragonite and calcite production has been shown to proceed via ACC (Fitzer et al., 2016), would indicate that the $+\Delta_{48}$ bias of ACC can be subsequently overprinted during its transformation to the final polymorph.

Based on the analysis of a single specimen we cannot identify which process is responsible for the apparent disequilibrium signal in RG2. We also need to bear in mind that we statistically expect one of the ~20 samples reported here to fall outside of its 95% confidence interval reflected by its measured mean value and fully propagated 2 SE. More dual clumped isotope data on intertidal species is required to investigate if their isotopic compositions are affected by kinetic isotope effects. While *M. gigas* as well as *M. edulis* also occur in intertidal habitats and therefore could help resolve this issue, there were no tidal cycles present during the time period of culture experiments in which these specimens were grown. Future studies using dual clumped isotopes should also confirm whether kinetic limitations occur in the inner shell layer, as postulated previously (Curley et al., 2023).

4.4 Oxygen isotope fractionation into aragonitic and calcitic mollusc shells

It is still unknown if, and to which extent, the temperature dependence of equilibrium oxygen isotope fractionation between aragonite and water differs from that between calcite and water. Attempts to determine such equilibrium relationships have been made using inorganic precipitation under controlled conditions (e.g., Kim & O'Neil, 1997; Kim et al., 2007a) and through theoretical calculations (e.g., Zheng, 1999; Hill et al., 2014). In the case of calcite, it has been demonstrated that it is hard to achieve isotopic equilibrium conditions during inorganic precipitation experiments. Contrary to the exclusive temperature control that is characteristic for the attainment of equilibrium conditions in the $CaCO_3$-DIC-H_2O system, it has been shown that the oxygen isotope fractionation also varied with pH (due to the kinetic isotope effects (KIE's) associated with CO_2-bicarbonate interconversion) and precipitation rate (e.g., Dietzel et al., 2009). Attainment of oxygen isotope equilibrium during aragonite precipitation experiments is even more challenging to accomplish since this polymorph is metastable at

ambient temperatures, such that calcite precipitation needs to be kinetically inhibited (e.g.) via the addition of Mg^{2+} (e.g., Kim et al., 2007a). Theoretically predicted temperature relationships for aragonite have large uncertainties and do often not confirm experimental results (see e.g., Zhou & Zheng, 2003 versus Kim et al., 2007a). In the case of calcite, it has been postulated that the indistinguishable relationships of Coplen (2007) and Däeron et al. (2019) represent the temperature dependence of oxygen isotope fractionation closest to equilibrium, as the investigated subaqueous calcites were precipitated at lowest possible natural rates (<1 µm/yr). In the temperature range of 0-40°C, these two calcitic $1000\ln\alpha$-1/T relationships differ from the proposed equilibrium relationship for aragonite after Kim et al. (2007a) by 0.8 to 1.0‰, supporting evidence for the theory that the two mineralogies are characterised by different states of equilibrium with respect to heterogeneous oxygen isotope fractionation relative to water. On the contrary, there is currently no indication from clumped isotope measurements that aragonite and calcite exhibit different states of clumped isotope equilibrium with respect to temperature (e.g., Defliese et al., 2015; de Winter et al., 2022). The majority of the molluscs analysed in this study are predominantly composed of calcite and exhibit dual clumped isotope compositions that are indistinguishable from the inorganic calcite equilibrium-Δ_{47}-Δ_{48}-T relationship of Fiebig et al. (2024), which, in its low temperature range, exclusively relies on the Devils Hole and Laghetto Basso samples that were also analysed by Coplen (2007) and Däeron et al. (2019). The temperature–Δ_{48} relationship presented by Swart et al. (2021) is indistinguishable to that of Fiebig et al., (2024), but was calibrated exclusively using synthetic carbonate precipitated as cold as 5°C. Even in the case of aragonite contribution, temperatures derived from measured Δ_{47} values agree with known habitat temperatures, supporting earlier evidence that calcite and aragonite may exhibit indistinguishable Δ_{47}-T equilibrium relationships (e.g., Defliese et al., 2015; de Winter et al., 2022).

Mollusc-specific $1000\ln\alpha(CaCO_3\text{-}H_2O)$-1/T relationships from compiled calcite and aragonite datasets are displayed in Figure 3a, b. These relationships are compared to the inorganic calcite

relationships proposed by Coplen (2007) and Kim & O'Neil (1997), and to the inorganic aragonite relationship by Kim et al. (2007a) in Figure 3c. We find that calcitic molluscs exhibit oxygen isotope fractionations closer to the equilibrium fractionation proposed by Coplen (2007) at warmer temperatures (Fig. 3c). On the contrary, at colder temperatures, the molluscan calcite fractionation line approaches the regression line published by Kim and O'Neil (1997). Over the investigated range of 0-40°C, at any given T, the oxygen isotope fractionation between aragonitic molluscs and seawater is 0.5 to 1.0‰ larger than that between calcitic molluscs and seawater (Fig. 3c). Aragonitic molluscs display the same behaviour as their calcitic counterparts; corresponding oxygen isotope fractionations approach values predicted by Coplen (2007) at the upper end of the temperature range covered by the data (~30°C), but increasingly deviate from the latter with decreasing temperature and approach the inorganic aragonite relationship published by Kim et al. (2007a). Our observation that the oxygen isotope fractionation between aragonite and water approaches values predicted by Coplen (2007) at elevated temperatures may indicate that aragonite and calcite share the same $1000\ln\alpha(CaCO_3\text{-}H_2O)\text{-}1/T$ equilibrium relationship, but that the attainment of isotopic equilibrium with water is kinetically inhibited at common Earth-surface temperatures. The observed differences in the magnitude of oxygen isotope fractionation between aragonite and calcite might be due to small differences in kinetic isotope effects (KIEs) prevalent at the mineral-fluid interface during mineral formation. These KIEs might differ in extent depending on the forming polymorph, for example, because detachment/attachment kinetics may depend on the symmetrical characteristics of the mineral surface which, in turn, may depend on the respective polymorph that is forming. Alternatively, the higher level of supersaturation required for aragonite precipitation may, for a given pH and temperature, proceed with faster interconversion between dissolved CO_2 and bicarbonate.

Above a temperature of 10°C, at which kinetic departures from Δ_{47} and Δ_{48} equilibrium values may become insignificant (Fig. 1), our empirical mollusc-specific $1000\ln\alpha(CaCO_3\text{-}H_2O)\text{-}1/T$

relationships for aragonite and calcite depart from that of Coplen (2007) by up to -0.5‰ and -1.2‰, respectively (Fig. 3c). This is large compared to the typical uncertainty of <0.1‰ for oxygen isotope analysis of carbonates and water and, therefore, confirms earlier indications that oxygen isotopes are more sensitive to kinetic effects than clumped isotopes (e.g., Kelson et al., 2017; Levitt et al., 2018; Jautzy et al., 2020; Fiebig et al., 2021). The observed discrepant behaviour between clumped and oxygen isotopes may support the hypothesis that interfacial isotopic equilibration occurs faster for clumped than for oxygen isotopes (Tripati et al., 2015; Levitt et al., 2018), such that there exists a precipitation regime where DIC disequilibrium is exclusively recorded in the oxygen isotope composition of the precipitated carbonate. Alternatively, it may simply indicate that clumped isotopes are less sensitive to interfacial kinetics than oxygen isotopes.

4.5 Application to fossil material – temperature and $\delta^{18}O_{sw}$ reconstructions for the mid-Eocene

Our modern mollusc shell data provide evidence that these carbonates represent robust archives for accurate and highly precise paleo-temperature reconstructions by means of exclusive Δ_{47} measurements, without the need for a mollusc-specific calibration relationship. As long as temperature exceeds 10°C such that significant kinetic isotope effects are absent, uncertainties in reconstructed temperatures are exclusively defined by the analytical uncertainty of Δ_{47} measurements. To test whether disequilibrium effects are similarly absent in fossil material, the dual clumped isotope signature of five Eocene mollusc shells collected from the same bed were measured (see Methods). As was the case for all modern samples with growth temperatures >10°C, all investigated fossil samples correspond to dual clumped isotope equilibrium within the uncertainty of the measurements (Fig. 2). Δ_{47}-derived temperatures are 17.3°C (±2.3°C, 95CI) for FG1, 20.5°C (±2.3°C, 95CI) for FG2, 20.3°C (±2.3°C, 95CI) for FG3, 20.7°C (±2.4°C, 95CI) for FM1, and 23.2°C (±2.3°C, 95CI) for FM2 (Table 4). A temperature of

23.3°C (±5.0°C, 2SD) has been obtained on an older sample (42.5 Ma versus 39 Ma) from the Hampshire Basin (Evans et al., 2018), based on Δ_{47} analysis of a shallow-dwelling (symbiont-bearing) large benthic foraminifera. Marchegiano and John (2022) reported a temperature range of 15-23°C based on Δ_{47} analysis of gastropods from the Naish Member of the Barton Clay Formation – the same member from which the samples reported here were collected. While the geologically-rapid evolution in the paleo-geography of this region in the (mid) Eocene (Clark et al., 2022; Kniest et al., 2024b) means that we cannot unambiguously ascribe the cooler mollusc versus foraminifera-derived temperatures to changing global climate (although these are nonetheless within uncertainty of each other), we note that this is consistent with Eocene cooling globally and in the North Atlantic (Bijl et al., 2009; Inglis et al., 2015, 2023).

Insertion of Δ_{47} derived temperatures in equation (2) yields seawater $\delta^{18}O$ values between -3.5‰ and -2.3‰ for the mid Eocene (Table 4). These low and variable $\delta^{18}O$ seawater values agree well with those reconstructed for the Hampshire Basin, Southern part of the North Sea, and the Paris Basin, based on a combination of $\delta^{18}O_{carb}$ and Δ_{47} data. Evans et al. (2018) analysed foraminiferal calcite from the Hampshire Basin and reported $\delta^{18}O$ seawater values of -4.14‰ for an age of 42.5 Ma. Marchegiano and John (2022) analysed gastropods from the Bartonian in the Hampshire Basin. Their reconstructed $\delta^{18}O$ seawater values for the Naish Member of the Barton Clay Formation ranged from -1 to -2.5 ‰ Kniest et al. (2024a), analysing a 40 Ma old bivalve mollusc shell, reconstructed $\delta^{18}O$ seawater values of -0.9 ‰ to -2.7 ‰ for the Paris Basin. They reported substantial spatiotemporal seawater $\delta^{18}O$ variations which they ascribed to re-occurring freshwater input. Kniest et al. (2024b), by means of Ba/Ca and $^{87}Sr/^{86}Sr$ analysis of Eocene bivalves (genera *Venericor* and *Crassatella*), independently confirmed substantial freshwater fluxes into parts of the Hampshire Basin during the mid-Eocene. Variable and negative seawater $\delta^{18}O$ around -2 ‰ have also been reported for the early Bartonian in the southern part of the North Sea (De Man et al., 2004). Altogether, our and these previous studies contribute to a coherent picture of relatively negative and variable seawater $\delta^{18}O$ in this region

during the mid-late Eocene. The driver of this has been suggested to be the local hydrographic regime (Kniest et al., 2024b), in particular the relatively enclosed nature of at least parts of this basin during some intervals of the Eocene coupled with river-derived freshwater input to the relatively nearshore environments from which many of these samples derive.

5. Conclusions

We used dual clumped isotope thermometry to demonstrate that the bulk shell of molluscs may constitute a promising archive for accurate and highly precise temperature reconstructions using the Δ_{47} proxy. Molluscs with growth temperatures ≥10°C plot indistinguishably from dual clumped isotope equilibrium, while their corresponding Δ_{47} values correspond within uncertainty to independently constrained habitat temperatures. Kinetic biases may become important at temperatures <10°C only. We ascribe the absence of significant kinetic isotope effects in the clumped isotope composition to precipitation from a closely equilibrated DIC pool. Close attainment of isotopic equilibrium in the DIC pool is facilitated by the relatively low pH (~7.6-7.8) of the EPF and utilisation of carbonic anhydrase, but apparently becomes ineffective at T < 10°C.

In addition, we presented revised empirical relationships for the temperature dependence of oxygen isotope fractionation between molluscan aragonite/calcite and water, integrating over multiple species and datasets. At relatively high temperatures, both relationships become indistinguishable from the proposed calcite-water equilibrium relationship of Coplen (2007) suggesting that calcite and aragonite may have indistinguishable states of equilibrium, but that ambient temperatures are typically too low to fully attain bulk oxygen isotope equilibrium. At these temperatures, oxygen isotopes seem to be more prone to disequilibrium biases than clumped isotopes, which we attribute to a higher sensitivity of oxygen isotopes to surface kinetic effects.

Finally, we showed that a set of well-preserved Eocene mollusc samples are also characterised by equilibrium dual clumped isotope compositions. We used corresponding Δ_{47} values to

reconstruct temperature and $\delta^{18}O_{sw}$ of the Hampshire Basin (UK) at ~39 Ma. Our reconstructed temperatures of 17.3-23.2°C based on five different species are all within uncertainty of each other. Reconstructed seawater $\delta^{18}O$ values of -3.5 to -2.3‰ agree well with previous estimates, adding to a body of evidence that suggests substantial (seasonal) freshwater input to at least parts of this basin during this time.

Acknowledgments

We thank C. Renker and M. Grimm for the identification of fossil and modern species analysed in this study. Sven Hofmann, M. Tagliavento and M. Schumann are acknowledged for their support during clumped isotope analysis. R. Petschick kindly provided XRD measurements. Aleksandra Bitner is thanked for providing White Sea mollusc specimens, Max Janse for providing the *T. squamosa* specimen. Rob Witbaard is thanked for providing *Mytilus edulis* specimens. This work was enabled through FI-948/13-1 granted to JF through the Koselleck-programme of the DFG. JF, AD, DE and WM also acknowledge funding through the VeWA consortium by the LOEWE program of the Hessen Ministry of Higher Education, Research and the Arts, Germany. NJW is supported by the Dutch Science Foundation (NOW) through a VENI fellowship (Grant nr. VI. Veni.222.354) and through the FWO Climate Prize by the Flemish Research Council. DE additionally acknowledges support from the Volkswagen Stiftung *Experiment!* initiative (award reference: A131440). Further, WM and JF acknowledge DFG-funding through MU 3739/6-1 and FI-948/15-1, respectively.

Appendix A. Supplementary Material

Supplementary Figure S1 provides a comparison of Δ_{47}/Δ_{48} values of unbleached (RG2_U), bleached RG2* and pooled RG2. Results of the applied bootstrapping approach (see Section 3) are shown in Supplementary Figure S2.

Compiled oxygen isotope data on molluscs and seawater and corresponding habitat temperatures are available in Supplementary Table S1. Baseline-corrected clumped isotope input data (δ^{45}-δ^{49}) as well as Δ_{47}, Δ_{48}, $\delta^{18}O$, and $\delta^{13}C$ results can be found in Supplementary Tables S2 (pooled over all RG2 aliquots) and S3 (RG2 and RG2_U aliquots evaluated separately), along with processing statistics.

Data Availability

All data is accessible from https://doi.org/10.5281/zenodo.14961836.

References

Arndt, I., Bernecker, M., Erhardt, T., Evans, D., Fiebig, J., Fursman, M., Kniest, J., Renema, W., Schlidt, V., Staudigel, P., Voigt, S., Müller, W., 2024. 20,000 days in the life of a giant clam reveal late Miocene tropical climate variability. Palaeogeography, Palaeoclimatology, Palaeoecology 661, 112711

Addadi, L., Raz, S., Weiner, S., 2003. Taking advantage of disorder: amorphous calcium carbonate and its roles in biomineralization. Advanced Materials 15, 959-970

Addadi, L., Joester, D., Nudelman, F., Weiner, S., 2006. Mollusk shell formation: A source of new concepte for understanding biomineralization process. Chemistry A European Journal 12, 980-987

Adkins, J. F., Boyle, E. A., Curry, W. B., Lutringer, A., 2003. Stable isotopes in deep-sea corals and a new mechanism for "vital effects". Geochimica et Cosmochimica Acta 67, 1129-1143

Affek, H. P., 2013. Clumped isotopic equilibrium and the rate of isotope exchange between CO_2 and water. American Journal of Science 313, 309-325

Affek, H. P., Matthews, A., Ayalon, A., Bar-Matthews, M., Burstyn, Y., Zaarur, S., Zilberman, T., 2014. Accounting for kinetic isotope effects in Soreq Cave (Israel) speleothems. Geochimica et Cosmochimica Acta 143, 303-318

Affek, H. P., Zaarur, S., 2014. Kinetic isotope effect in CO_2 degassing: Insight from clumped and oxygen isotopes in laboratory precipitation experiments. Geochimica et Cosmochimica Acta 143, 319-330

Anderson, N. T., Kelson, J. R., Kele, S., Daëron, M., Bonifacie, M., Horita, J., Mackey T. J., John, C. M., Kluge, T., Petschnig, P., Jost, A. B., Huntington, K. W., Bernasconi, S. M., Bergmann, K. D., 2021. A Unified Clumped Isotope Thermometer Calibration (0.5-1,100°C) Using Carbonate-Based Standardization. Geophysical Research Letters 48:7, e2020GL092069

Bajnai, D., Fiebig, J., Tomasovych, A., Milner Garcia, S., Rollion-Bard, C., Raddatz, J., Löffler, N., Primo-Ramos, C., Brand, U., 2018. Assessing kinetic fractionation in brachiopod calcite using clumped isotopes. Scientific Reports 8:533 (DOI:10.1038/s41598-017-17353-7)

Bajnai, D., Guo, W., Löffler, N., Methner, K., Krsnik, E., Coplen, T. B., Gischler, E., Hansen, M., Henkel, D., Price, G. D., Raddatz, J., Scholz, D., Fiebig, J., 2020. Combined clumped isotope measurements resolve kinetic biases in carbonate formation temperatures. Nature Communications 11:4005

Batenburg, S. J., Reichart, G.-J., Jilbert, T., Janse, M., Wesselingh, F. P., Renema, W., 2011. Interannual climate variability in the Miocene: High resolution trace element and stable isotope ratios in giant clams. Palaeogeography, Palaeoclimatology, Palaeoecology 306, 75-81

Bernasconi, S. M., Müller, I. A., Bergmann, K. D., Breitenbach, S. F. M., Fernandez, A., Hodell, D. A., Jaggi, M., Meckler, A. N., Millan, I., Ziegler, M., 2018. Reducing uncertainties

in carbonate clumped isotope analysis through consistent carbonate-based standardization. Geochemistry, Geophysics, Geosystems 19:9, 2895-2914

Bernecker, M., Hofmann, S., Staudigel, P.T., Davies, A.J., Tagliavento, M., Meijer, N., Ballian, A., Fiebig, J., 2023. A robust methodology for triple (Δ_{47}, Δ_{48}, Δ_{49}) clumped isotope analysis of carbonates. Chemical Geology 642, 121803

Bertucci, A., Moya, A., Tambutté, S., Allemand, D., Supuran, C. T., Zoccola, D., 2013. Carbonic anhydrases in anthozoan corals – A review. Bioorganic & Medical Chemistry 21, 1437-1450

Bijl, P. K., Schouten, S., Sluijs, A., Reichart, G.-J., Zachos, J. C., Brinkhuis, H., 2009. Early Palaeogene temperature evolution of the southwest Pacific Ocean. Nature 461, 776-779

Burnett, L. E., 1988. Physiological responses to air exposure: acid-base balance and the role of branchial water stores. Amer. Zool. 28, 125-135

Butler, P. G., Wanamaker, A. D., Scourse, J. D., Richardson, C. A., and Reynolds, D. J., 2013. Variability of marine climate on the North Icelandic Shelf in a 1357-year proxy archive based on growth increments in the bivalve Arctica islandica. Palaeogeography, Palaeoclimatology, Palaeoecology, 373, 141–151

Caldarescu, D. E., Sadatzki, H., Andersson, C., Schäfer, P., Fortunato, H., Meckler, A. N., 2021. Clumped isotope thermometry in bivalve shells: A tool for reconstructing seasonal upwelling. Geochimica et Cosmochimica Acta 294, 174-191

Cardoso, J. C. R., Ferreira, V., Zhang, X., Anjos, L., Félix, R. C., Batista, F. M., Power, D. M., 2019. Evolution and diversity of alpha-carbonic anhydrases in the mantle of the Mediterranean mussel (Mytilus galloprovincialis). Scientific Reports 9, 10400

Carré, M., Bentaleb, I., Bruguier, O., Ordinola, E., Barrett, N. T., Fontugne, M., 2006. Calcification rate influence on trace element concentrations in aragonitic bivalve shells: Evidences and mechanisms. Geochimica et Cosmochimica Acta 70, 4906-4920

Chen, S., Gagnon, A. C., Adkins, J. F., 2018. Carbonic anhydrase, coral calcification and a new model of stable isotope vital effects. Geochimica et Cosmochimica Acta 236, 179-197

Clark, A. J., Vellekoop, J., Speijer, R. P., 2022. Hydrological differences between the Lutetian Paris and Hampshire basins revealed by stable isotopes of conid gastropods, Bulletin de la Société Géologique de France, 193, 3

Coplen, T. B., 2007. Calibration of the calcite-water oxygen-isotope geothermometer at Devils Hole, Nevada, a natural laboratory. Geochimica et Cosmochimica Acta 71, 3948-3957

Crenshaw, M. A., 1972. The soluble matrix of Mercenaria mercenaria shell. Biomineralization 6, 6-11

Curley A. N., Petersen S. V., Stewart M. E., Guo W. 2023. Biologically driven isotopic fractionations in bivalves: from paleoenvironmental problem to palaeophysiological proxy. Biological Reviews 98, 1016-1032

Daëron, M., Guo, W., Eiler, J., Genty, D., Blamart, D., Boch, R., Drysdale, R., Maire, R., Wainer, K., Zanchetta, G., 2011. $^{13}C^{18}O$ clumping in speleothems: Observations from natural caves and precipitation experiments. Geochimica et Cosmochimica Acta 75, 3303-3317

Daëron, M., Drysdale, R. N., Peral, M., Hyughe, D., Blamart, D., Coplen, T. B., Lartaud, F., Zanchetta, G., 2019. Most Earth-surface calcites precipitate out of isotopic equilibrium. Nature Communications 10:429

Daëron, M., 2021. Full Propagation of Analytical Uncertainties in Δ_{47} Measurements. Geochemistry, Geophysics, Geosystems 22:5

Davies, A. J., John, C. M., 2019. The clumped (^{13}C-^{18}O) isotope composition of echinoid calcite: Further evidence for "vital effects" in the clumped isotope proxy. Geochimica et Cosmochimica Acta 245, 172-189

Davies, A. J., Davis, S., John, C. M., 2021. Evidence of taxonomic non-equilibrium effects in the clumped isotope composition of modern cephalopod carbonate. Chemical Geology 578, 120317

Davies, A. J., Guo, W., Bernecker, M., Tagliavento, M., Raddatz, J., Gischler, E., Flögel, S., Fiebig, J., 2022. Dual clumped isotope thermometry of coral carbonate. Geochimica et Cosmochimica Acta 338, 66-78

Davies, A. J., Brand, U., Tagliavento, M., Bitner, M. A., Bajnai, D., Staudigel, P. T., Bernecker, M., Fiebig, J., 2023. Isotopic disequilibrium in brachiopods disentangled with dual clumped isotope thermometry. Geochimica et Cosmochimica Acta 359, 135-147

Defliese, W. F., Hren, M. T., Lohmann, K. C., 2015. Compositional and temperature effects of phosphoric acid fractionation on Δ_{47} analysis and implications for discrepant calibrations. Chemical Geology 396, 51-60

De Man, E., Ivany, L., Vandenberghe, N., 2004. Stable oxygen isotope record of the Eocene-Oligocene transition in the southern North Sea Basin: positioning the Oi-1 event. Netherlands. Journal of Geosciences / Geologie en Mijnbouw 83, 193-197

Dennis, K. J., Affek, H. P., Passey, B. H., Schrag, D. P., Eiler, J. M., 2011. Defining an absolute reference frame for 'clumped' isotope studies of CO_2. Geochimica et Cosmochimica Acta 75, 7117-7131

de Winter, N. J., Vellekoop, J., Clark, A. J., Stassen, P., Speijer, R., Claeys, P., 2020. The giant marine gastropod Campanile giganteum (Lamarck, 1804) as a high-resolution archive of seasonality in the Eocene greenhouse world. Geochemistry, Geophysics, Geosystems 21:4, e2019GC008794

de Winter, N. J., Dämmer, L. K., Falkenroth, M., Reichart, G.-J., Moretti, S., Martínez-García, A., Höche, N., Schöne, B. R., Rodiouchkina, K., Goderis, S., Vanhaecke, F., van Leeuwen, S. M., and Ziegler, M., 2021a. Multi-isotopic and trace element evidence against different formation pathways for oyster microstructures, Geochimica et Cosmochimica Acta, 308, 326–352, https://doi.org/10.1016/j.gca.2021.06.012

de Winter, N. J., Agterhuis, T., Ziegler, M., 2021b.: Optimizing sampling strategies in high-resolution paleoclimate records, Climate of the Past 17, 1315–1340.

de Winter, N. J., Witbaard, R., Kocken, I. J., Müller, I. A., Guo, J., Goudsmit, B., Ziegler, M., 2022. Temperature dependence of clumped isotopes (Δ_{47}) in aragonite. Geophysical Research Letters 49, e2022GL099479

Dietzel, M., Tang, J., Leis, A., Köhler S. J., 2009. Oxygen isotopic fractionation during inorganic calcite precipitation – effects of temperature, precipitation rate and pH. Chemical Geology 268, 107-115

Evans, D., Sagoo, N., Renema, W., Cotton, L. J., Müller, W., Todd, J. A., Saraswati, P. K., Stassen, P., Ziegler, M., Pearson, P. N., Valdes, P. J., Affek, H. P., 2018. Eocene greenhouse climate revealed by coupled clumped isotope-Mg/Ca thermometry. Proceedings of the National Academy of Sciences USA 115, 1174-1179.

Fiebig, J., Bajnai, D., Löffler, N., Methner, K., Krsnik, E., Mulch, A., Hofmann, S., 2019. Combined high-precision Δ_{48} and Δ_{47} analysis of carbonate. Chemical Geology 522, 186-191

Fiebig, J., Daeron, M., Bernecker, M., Guo, W., Schneider, G., Boch, R., Bernasconi, S. M., Jautzy, J., Dietzel, M., 2021. Calibration of the dual clumped isotope thermometer for carbonates. Geochimica et Cosmochimica Acta 312, 235-256

Fiebig, J., Bernecker, M., Meijer, N., Methner, K., Staudigel, P. T., Davies, A. J., Bayarjargal, L., Spahr, D., Winkler, B., Hofmann, S., Granzin, M., Petersen, S. V., 2024. Carbonate clumped isotope values compromised by nitrate-derived NO_2 interferent. Chemical Geology 670: 122382

Fitzer, S. C., Chung, P., Maccherozzi, F., Dhesi, S. S., Kamensos, N. A., Phoenix, V. R., Cusack, M., 2016. Biomineral shell formation under ocean acidification: a shift from order to chaos. Scientific Reports 6, 21076

Freeman, J. A., Willbur, K. M., 1948. Carbonic anhydrase in molluscs. The Biological Bulletin 94, 55-59

Ghosh, P., Adkins, J., Affek, H., Balta, B., Guo, W., Schauble, E. A., Schrag, D., Eiler, J. M., 2006. ^{13}C-^{18}O bonds in carbonate minerals: A new kind of paleothermometer. Geochimica et Cosmochimica Acta 70, 1439-1456

Goodwin, D. H., Flessa, K. W., Schöne, B. R., and Dettman, D. L.: Cross-calibration of daily growth increments, stable isotope variation, and temperature in the Gulf of California bivalve mollusk Chione cortezi: implications for paleoenvironmental analysis, Palaios, 16, 387–398, 2001.

Grossman, E. L., Ku, T.-L., 1986. Oxygen and carbon isotope fractionation in biogenic aragonite: temperature effects. Chemical Geology 59, 59-74

Guo, W., 2020. Kinetic clumped isotope fractionation in the DIC-H_2O-CO_2 system: Patterns, controls, and implications. Geochimica et Cosmochimica Acta 268, 230-257

Guo, W., Zhou, C., 2019. Patterns and controls of disequilibrium isotope effects in speleothems: Insights from an isotope-enabled diffusion-reaction model and implications for quantitative thermometry. Geochimica et Cosmochimica Acta 267, 196-226

Harwood, A. J. P., Dennis, P. F., Marca, A. D., Pilling, G. M., Millner, R. S., 2008. The oxygen isotope composition of water masses within the North Sea. Estuarine, Coastal and Shelf Science 78, 353-359

Henkes, G. A., Passey, B. H., Wanamaker Jr., A. D., Grossman, E. L., Ambrose Jr., W. G., Carroll, M. L., 2013. Carbonate clumped isotope compositions of modern marine mollusc and brachiopod shells. Geochimica et Cosmochimica Acta 106, 307-325

Hill, P. S., Tripati, A. K., Schauble, E. A., 2014. Theoretical constraints on the effects of pH, salinity, and temperature on clumped isotope signatures of dissolved inorganic carbon species and precipitating carbonate minerals. Geochimica et Cosmochimica Acta 125, 610-651

Huyghe, D., Lartaud, F., Emmanuel, L., Merle, D., and Renard, M.: Palaeogene climate evolution in the Paris Basin from oxygen stable isotope ($\delta^{18}O$) compositions of marine molluscs, Journal of the Geological Society, 172, 576–587, 2015.

Huyghe, D., Daeron, M., de Rafelis, M., Blamart, D., Sébilo, M., Paulet, Y.-M., Lartaud, F., 2022. Clumped isotopes in modern marine bivalves. Geochimica et Cosmochimica Acta 316, 41-58

Immenhauser, A., Schöne, B. R., Hoffmann, R., Niedermayr, A., 2016. Mollusc and brachiopod skeletal hard parts: Intricate archives of their marine environment. Sedimentology 63, 1-59

Inglis, G. N., Farnsworth, A., Lunt, D., Foster, G. L., Hollis, C. J., Pagani, M., Jardine, P. E., Pearson, P. N., Markwick, P., Galsworthy, A. M. J., Raynham, L., Taylor, K. W. R., Pancost, R. D., 2015. Descent toward the Icehouse: Eocene sea surface cooling inferred from GDGT distributions. Paleoceanography 30, 1000-1020

Inglis, G. M, Bhatia, R., Evans, D., Zhu, J., Müller, W., Mattey, D., Thornalley, D. J. R., Stockey, R. G., Wade, B. S., 2023. Surface ocean cooling in the Eocene North Atlantic coincides with declining atmospheric CO_2. Geophysical Research Letters 50:24, e2023GL105448

Ip, Y. K., Loong, A. M., Hiong, K. C., Wong, W. P., Chew, S. F., Reddy, K., Sivaloganathan, B., Ballantyne, J. S., 2006. Light induces an increase in the pH of and a decrease in the ammonia concentration in the extrapallial fluid of the giant clam Tridacna squamosa. Physiological and Biochemical Zoology 79, 656-664

Ivany, L.C., Judd, E.J., 2022. Deciphering Temperature Seasonality in Earth's Ancient Oceans. Annual Review of Earth and Planetary Sciences, 50, 123–152.

Jacob, D. E., Wirth, R., Soldati, A. L., Wehrmeister, U., Schreiber, A. 2011. Amorphous calcium carbonate in the shells of adult *Unionoida*. Journal of Structural Biology 173:2, 241-249

Janse, M., Wensing, J., Gieling, H., de Jongh, T., Leewis, R., 2008. Ecological management of a large coral reef eco-display at Burgers' Zoo, Arnhem, The Netherlands. *Advances in Coral Husbandry in Public Aquariums Public Aquarium Husbandry Series, eds RJ Leewis and M. Janse (Arnhem: Burgers' Zoo)*, pp.293-303.

Jansen, J. M., Pronker, A. E., Kube, S., Sokolowski, A., Sola, J. C., Marquiegui, M. A., Schiedek, D., Bonga, S. W., Wolowicz, M., Hummel, H., 2007. Geographic and seasonal patterns and limits on the adaptive response to temperature of European *Mytilus* spp. and *Macoma balthica* populations. Oecologia 154, 23-34

Jautzy, J., Savard, M., Dhillon, R., Bernasconi, S., Lavoie, D., Smirnoff, A., 2020. Clumped isotope temperature calibration for calcite: Bridging theory and experimentation. Geochemical Perspective Letters 14, 36-41

Judd, E. J., Wilkinson, B. H., and Ivany, L. C., 2017. The life and time of clams: Derivation of intra-annual growth rates from high-resolution oxygen isotope profiles. Palaeogeography, Palaeoclimatology, Palaeoecology 490, 70-83

Judd, E. J., Tierney, J. E., Lunt, D. J., Montañez, I. P., Huber, B. T., Wing, S. L., and Valdes, P. J., 2024. A 485-million-year history of Earth's surface temperature. Science 385, eadk3705

Kaandorp, R. J. G., Vonhof, H. B., Del Busto, C., Wesselingh, F. P., Ganssen, G. M., Marmól, A. E., Romero Pittman, L., and van Hinte, J. E., 2003. Seasonal stable isotope variations of the modern Amazonian freshwater bivalve *Anodontites trapesialis*. Palaeogeography, Palaeoclimatology, Palaeoecology 194, 339–354

Kelson, J. R., Huntington, K. W., Schauer, A. J., Saenger, C., Lechler, A. R., 2017. Toward a universal carbonate clumped isotope calibration: Diverse synthesis and preparatory methods suggest a single temperature relationship. Geochimica et Cosmochimica Acta 197, 104-131

Kim, S.-T., O'Neil, J. R., 1997. Equilibrium and nonequilibrium oxygen isotope effects in synthetic carbonates. Geochimica et Cosmochimica Acta 61, 3461-3475

Kim, S.-T., Mucci, A., Taylor, B. E., 2007a. Phosphoric acid fractionation factors for calcite and aragonite between 25 and 75°C: Revisited. Chemical Geology 246, 135-146

Kim, S.-T., O'Neil, J. R., Hillaire-Marcel, C., Mucci, A., 2007b. Oxygen isotope fractionation between synthetic aragonite and water: Influence of temperature and Mg^{2+} concentration. Geochimica et Cosmochimica Acta 71, 4704-4715

Kniest, J. F., Davies, A. J., Brugger, J., Fiebig, J., Bernecker, M., Todd, J. A., Hickler, T., Voigt, S., Woodland, A., Raddatz, J., 2024a. Dual clumped isotopes from the Mid-Eocene bivalve shell reveal a hot and summer wet climate of the Paris Basin. Communications Earth & Environment 5: 330

Kniest, J. F., Evans, D., Gerdes, A., Cantine, M., Todd, J. A., Sigwart, J. D., Vellekoop, J., Müller, W., Voigt, S., Raddatz, J., 2024b. Spatiotemporal changes in riverine input into the Eocene North Sea revealed by strontium isotope and barium analysis of bivalve shells. Scientific Reports 14: 28806

Lécuyer, C., Hutzler, A., Amiot, R., Daux, V., Grosheny, D., Otero, O., Martineau, F., Fourel, F., Balter, V., Reynard, B., 2012. Carbon and oxygen isotope fractionations between aragonite and calcite of shells from modern molluscs. Chemical Geology 332-333, 92-101

Lécuyer, C., Reynard, B., Martineau, F., 2004. Stable isotope fractionation between mollusc shells and marine waters from Martinique Island. Chemical Geology 213, 293-305

Le Roy, N., Jackson, D. J., Marie, B., Ramos-Silva, P., Marin, F., 2016. Carbonic anhydrase and metazoan biocalcification: A focus on molluscs. Key Engineering Materials 672, 151.157

Levitt, N., P., Eiler, J. M., Romanek, C. S., Beard, B. L., Xu, H., Johnson, C. M., 2018. Near equilibrium ^{13}C-^{18}-O bonding during inorganic calcite precipitation under chemo-stat conditions. Geochemistry, Geophysics, Geosystems 19, 901-920

Levitus, S., Boyer, T.P, Garcia, H.E., Locarnini, R.A., Zweng, M.M., Mishonov, A.V., Reagan, J.R., Antonov, J.I., Baranova, O.K., Biddle, M., Hamilton, M., Johnson, D.R., Paver, C.R., Seidov, D. (2015). World Ocean Atlas 2013 (NCEI Accession 0114815). [Temperature dataset]. NOAA National Centers for Environmental Information. Dataset. https://doi.org/10.7289/v5f769gt

Lindinger, M. I., Lauren, D. J., McDonald, D. G., 1984. Acid-base-balance in the sea mussel, Mytilus edulis. 3. Effects of environmental hypercapnia on intracellular and extracellular acid-base-balance. Marine Biology Letters 5, 371-381

Locarnini, R.A., Mishonov, A.V., Antonov, J.I.,, Boyer, T.P., Garcia, H.E.,, Baranova, O.K., Zweng,, M.M., Johnson, D.R., 2010. *World Ocean Atlas 2009, Volume 1: Temperature*. S. Levitus, Ed. NOAA Atlas NESDIS 68, U.S. Government Printing Office, Washington, D.C., 184 pp.

Lu, C., Murray, S.T., Klaus, J., McNeill, D.F., Swart, P.K. (2024) Dual clumped isotopes ((Δ_{47} and Δ_{48}) reveal non-equilibrium formation of freshwater cements. Geochimica et Cosmochimica Acta 379, 145-157.

Lu, C.L., Swart, P.K., (2024) The application of dual clumped isotope thermometer ((Δ_{47} and Δ_{48}) to the understanding of dolomite formation. Geology 52, 56-60.

Marchegiano, M., John, C. M., 2022. Disentangling the impact of global and regional climate changes during the Middle Eocene in the Hampshire Basin: New insights from carbonate clumped isotopes and ostracod assemblages. Paleoceanography and Paleoclimatology 37, e2021PA004299

Marie, B., Luquet, G., Bédouet, L., Milet, C., Guichard, N., Medakovic, D., Marin, F., 2008. Nacre Calcification in the Freshwater Mussel *Unio pictorium*: Carbonic Anhydrase Activity and Purificaion of a 95 kDa Calcium-Binding Glycoprotein. ChemBioChem 9, 2515-2523

McConnaughey, T., 1989a. ^{13}C and ^{18}O disequilibrium in biological carbonates: I. Patterns. Geochimica et Cosmochimica Acta 53, 151-162

McConnaughey, T., 1989b. ^{13}C and ^{18}O isotopic disequilibrium in biological carbonates: II. *In vitro* simulation of kinetic isotope effects. Geochimica et Cosmochimica Acta 53, 163-171

Miyamoto, H., Miyashita, T., Okushima, M., Nakano, S., Morita, T., Matsushiro, A., 1996. A carbonic anhydrase from the nacreous layer in oyster pearls. Proceedings of the National Academy of Sciences USA 93, 9657-9660

Miyamoto, H., Miyoshi, F., Kohno, J., 2005. The carbonic anhydrase domain protein nacrein is expressed in the epithelial cells of the mantle and acts as a negative regulator in calcification in the mollusk Pinctada fucata. Zoological Science 22, 311-315

Nassif, N., Pinna, N., Gehrke, N., Antonietti, M., Jäger, C., Cölfen H., 2005. Amorphous layer around aragonite platelets in nacre. Proceedings of the National Academy of Sciences USA 102, 36, 12653-12655

Nehrke, G., Poigner, H., Wilhelms-Dick, D., Brey, T., Abele, D., 2012. Coexistencew of three calcium carbonate polymorphs in the shell of the Antarctic clam Laternula elliptica. Geochemistry, Geophysics, Geosystems 13:5

Nielsen, S. A., Frieden, E., 1972. Carbonic anhydrase activity in molluscs. Comparative Biochemistry and Physiology 41B, 461-468

Nooitgedacht, C. W., van der Lubbe, H. J. L., Ziegler, M., Staudigel, P. T., 2021. Internal water facilitates thermal resetting of clumped isotopes in biogenic aragonite. Geochemistry, Geophysics, Geosystems 22, e2021GC009730

Park, D.-K., Lee, M. S., 2019. Kinetic study of catalytic CO_2 hydration by metal-substituted biomimetic carbonic anhydrase model complexes. Royal Society Open Science 6:190407.

Parvez, Z.A., Lucarelli, J.K., Matamaros, I.W., Rubi, J., Miguel, K., Elliott, B., Flores, R., Ulrich, R.N., Eagle, R.A., Watkins, J.M., Christensen, J.N., Tripati, A., 2023. Dual carbonate clumped isotopes (Δ_{47}-Δ_{48}) constrains kinetic effects and timescales in peridotite-associated springs at the Cedars, Northern California. Geochimica et Cosmochimica Acta 358, 77-92.

Parvez, Z.A., El-Shenawy, M., Lucarelli, J.K., Kim, S.T., Johnson, K.R., Wright, K., Gebregiorgis, D., Montanez, I.P., Wortham, B., Asrat, A., Reinhardt, E., Christensen, J.N., Matamoros, I.W., Rubi, J., Miguel, K., Elliott, B.M., Flores, R., Kovacs, S., Eagle, R.A., Tripati, A., 2024. Dual carbonate clumped isotope ((Δ_{47}-Δ_{48}) measurements constrain different sources of kinetic isotope effects and quasi-equilibrium signatures in cave carbonates. Geochimica et Cosmochimica Acta 366, 95-112.

Payne, J.L., Heim, N.A., Knope, M.L., McClain, C.R., 2014. Metabolic dominance of bivalves predates brachiopod diversity decline by more than 150 million years. Proceedings of the Royal Society B 281, 20133122.

Pederson, C., Mavromatis, V., Dietzel, M., Rollion-Bard, C., Nehrke, G., Jöns, N., Jochum, K. P., Immenhauser, A., 2019. Diagenesis of mollusc aragonite and the role of fluid reservoirs. Earth and Planetary Science Letters 514, 130-142

Ross, C. L., Warnes, A., Comeau, S., Cornwall, C. E., Cuttler, M. V. W., Naugle, M., McCulloch, M. T., Schoepf, V., 2022. Coral calcification mechanisms in a warming ocean and the interactive effects of temperature and light. Communications Earth and Environment 3:72

Sade, Z., Halevy, I., 2017. New constraints on kinetic isotope effects during CO_2(aq) hydration and hydroxylation: Revisiting theoretical and experimental data. Geochimica et Cosmochimica 214, 246-265

Saenger, C., Affek, H. P., Felis, T., Thiagarajan, N., Lough, J. M., Holcomb, M., 2012. Carbonate clumped isotope variability in shallow water corals: Temperature dependence and growth-related vital effects. Geochimica et Cosmochimica Acta 99, 224-242

Saenger, C., Gabitov, R. I., Farmer, J., Watkins, J. M., Stone, R., 2017. Linear correlations in bamboo coral $\delta^{13}C$ and $\delta^{18}O$ sampled by SIMS and micromill: Evaluating paleoceanographic potential and biomineralization mechanisms using $\delta^{11}B$ and Δ_{47} composition. Chemical Geology 454, 1-14

Schmidt, G.A., G. R. Bigg and E. J. Rohling. 1999. "Global Seawater Oxygen-18 Database - v1.22" https://data.giss.nasa.gov/o18data/

Schöne, B. R., Fiebig, J., Pfeiffer, M., Gleβ, R., Hickson, J., Johnson, A. L., Dreyer, W., Oschmann, W., 2005. Climate records from a bivalved Methuselah (*Arctica islandica*, Mollusca; Iceland), Palaeogeography, Palaeoclimatology, Palaeoecology, 228, 130–148

Spooner, P. T., Guo, W., Robinson, L. F., Thiagarajan, N., Hendry, K. R., Rosenheim, B. E., Leng, M. J., 2016. Clumped isotope composition of cold-water corals: A role for vital effects? Geochimica et Cosmochimica Acta 179, 123-141

Staudigel, P. T., Pederson, C., van der Lubbe, J., Bernecker, M., Tagliavento, M., Davies, A. J., Immenhauser, A., Fiebig, J. (2023a). An isotopologue-enabled model (Δ_{47}, Δ_{48}) for describing thermal fluid-carbonate interaction in open and closed diagenetic systems. Geochemistry, Geophysics, Geosystems 24, e2023GC011117.

Staudigel, P., Davies, A.J., Bernecker, M., Tagliavento, M., van der Lubbe, H.J.L., Nooitgedacht, C., Looser, N., Bernasconi, S.M., Vonhof, H., Price, G., Fiebig, J. (2023b) Fingerprinting kinetic isotope effects and diagenetic exchange reactions using fluid inclusion and dual-clumped isotope analysis. Geochemistry, Geophysics, Geosystems 24, e2022GC010766.

Staudigel, P. T., Feng, D., Peckmann, J., Bernecker, M., Davies, A. J., Tagliavento, M., Fiebig, J., 2024. Resolving and correcting for kinetic biases on methane seep paleotemperature using carbonate Δ_{47}/Δ_{48} analysis. Science Advances 10, eadn0155.

Swart, P.K., Lu, C., Moore, E.W., Smith, M.E., Murray, S.T., Staudigel, P.T. (2021) A calibration equation between Δ_{48} values of carbonate and temperature. Rap. Commun. Mass Spectrom. 35, e9147.

Tagliarolo, M., Grall, J., Chavaud, L., Clavier, J., 2013a. Aerial and underwater metabolism of Patella vulgata L.: comparison of three intertidal levels. Hydrobiologia 702, 241-253

Tagliarolo, M., Clavier, J., Chauvaud, L., Grall, J., 2013b. Carbon emission associated with respiration and calcification of nine gastropod species from the intertidal rocky shore of Western Europe. Marine Biology 160, 2891-2901

Tagliavento, M., Davies, A. J., Bernecker, M., Staudigel, P. T., Dawson, R. R., Dietzel, M., Götschl, K., Guo, W., Schulp, A. S., Therrien, F., Zelenitsky, D. K., Gerdes, A., Müller, W., Fiebig, J., 2023. Evidence for heterothermic endothermy and reptile-like eggshell mineralization in Troodon, a non-avian maniraptoran theropod. Proceedings of the National Academy of Sciences USA 120, e2213987120

Thiagarajan, N., Adkins, J., Eiler, J., 2011. Carbonate clumped isotope thermometry of deep-sea corals and implications for vital effects. Geochimica et Cosmochimica Acta 75, 4416-4425

Tripati, A. K., Hill, P. S., Eagle, R. A., Mosenfelder, J. L., Tang, J., Schauble, E. A., Eiler, J. M., Zeebe, R. E., Uchikawa, J., Coplen, T. B., Ries, J. B., Henry, D., 2015. Beyond temperature: Clumped isotope signatures in dissolved inorganic carbon species and the influence of solution chemistry on carbonate mineral composition. Geochimica et Cosmochimica Acta 166, 344-371

Uchikawa, J., Zeebe, R. E., 2012. The effect of carbonic anhydrase on the kinetics and equilibrium of the oxygen isotope exchange in the CO_2-H_2O system: Implications for $\delta^{18}O$ vital effects in biogenic carbonates. Geochimica et Cosmochimica Acta 95, 15-34

Venn, A. A., Tambutté, E., Caminti-Segonds, N., Techer, N., Allemand, D., Tambutté, S., 2019. Effects of light and darkness on pH ragulation in three coral species exposed to seawater acidification. Scientific Reports 9:2201

Vihtakari, M., Renaud, P. E., Clarke, L. J., Whitehouse, M. J., Hop, H., Carroll, M. L., Ambrose Jr, W. G., 2016. Decoding the oxygen isotope signal for seasonal growth patterns in Arctic bivalves. Palaeogeography, Palaeoclimatology, Palaeoecology 446, 263-283

Weber, J.N., Woodhead P.M.J., 1972. Temperature dependence of oxygen-18 concentration in reef coral carbonates. Journal of Geophysical Research 77, 463–473

Weiss I. M., Tuross N., Addadi L., Weiner S., 2002. Mollusc Larval Shell Formation: Amorphous Calcium Carbonate is a Precursor Phase for Aragonite. Journal of Experimental Zoology 293, 478–491

White, J. H., Defliese, W. F., 2023. $\delta^{13}C$ and $\delta^{18}O$ heterogeneities in carbonates: Nonlinear mixing in the application of dual-carbonate-clumped isotope thermometer. Rapid Communications in Mass Spectrometry 37, e9627

Witbaard, R., Jenness, M. I., Van Der Borg, K., and Ganssen, G., 1994. Verification of annual growth increments in Arctica islandica L. from the North Sea by means of oxygen and carbon isotopes. Netherlands Journal of Sea Research, 33, 91–101

Zheng, Y.-F., 1999. Oxygen isotope fractionation in carbonate and sulfate minerals. Geochemical Journal 33, 109-126

1050 Zhou, G.-T., Zheng, Y.-F., 2003. An experimental study of oxygen isotope fractionation
1051 between inorganically precipitated aragonite and water at low temperatures. Geochimica et
1052 Cosmochimica Acta 67:3, 387-399

1053

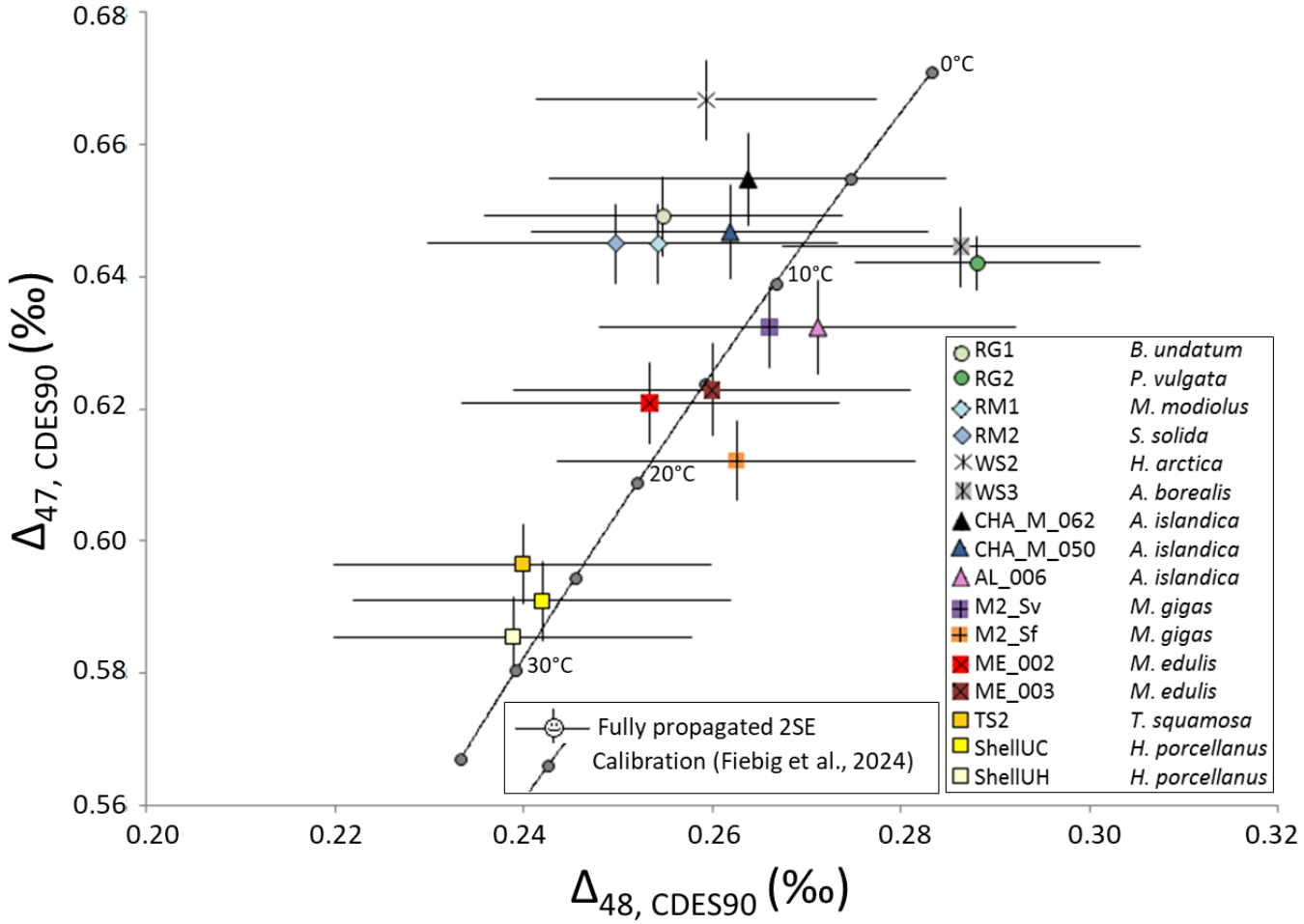

Fig. 1. Dual clumped isotope composition of modern molluscs.

Δ_{47}/Δ_{48} values of all modern samples are shown relative to the position of equilibrium (Fiebig et al., 2024). Respective error bars indicate fully propagated 2SE.

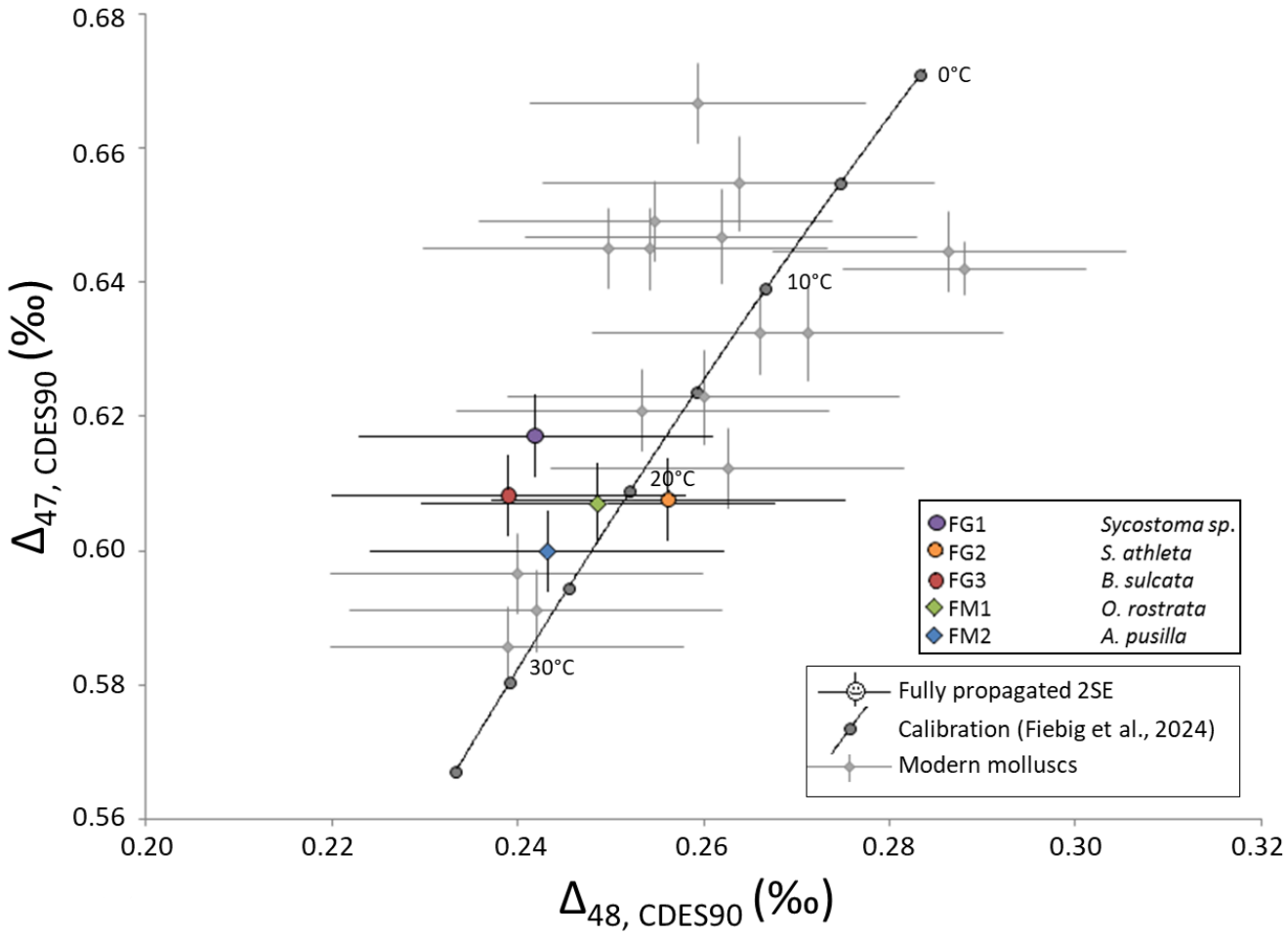

Fig. 2. Dual clumped isotope composition of Eocene molluscs.

Δ_{47}/Δ_{48} values of our five Eocene samples (solidly coloured circles and diamonds) are shown relative to the position of equilibrium (Fiebig et al., 2024). Modern molluscs are depicted in grey for comparison. Error bars indicate fully propagated 2SE.

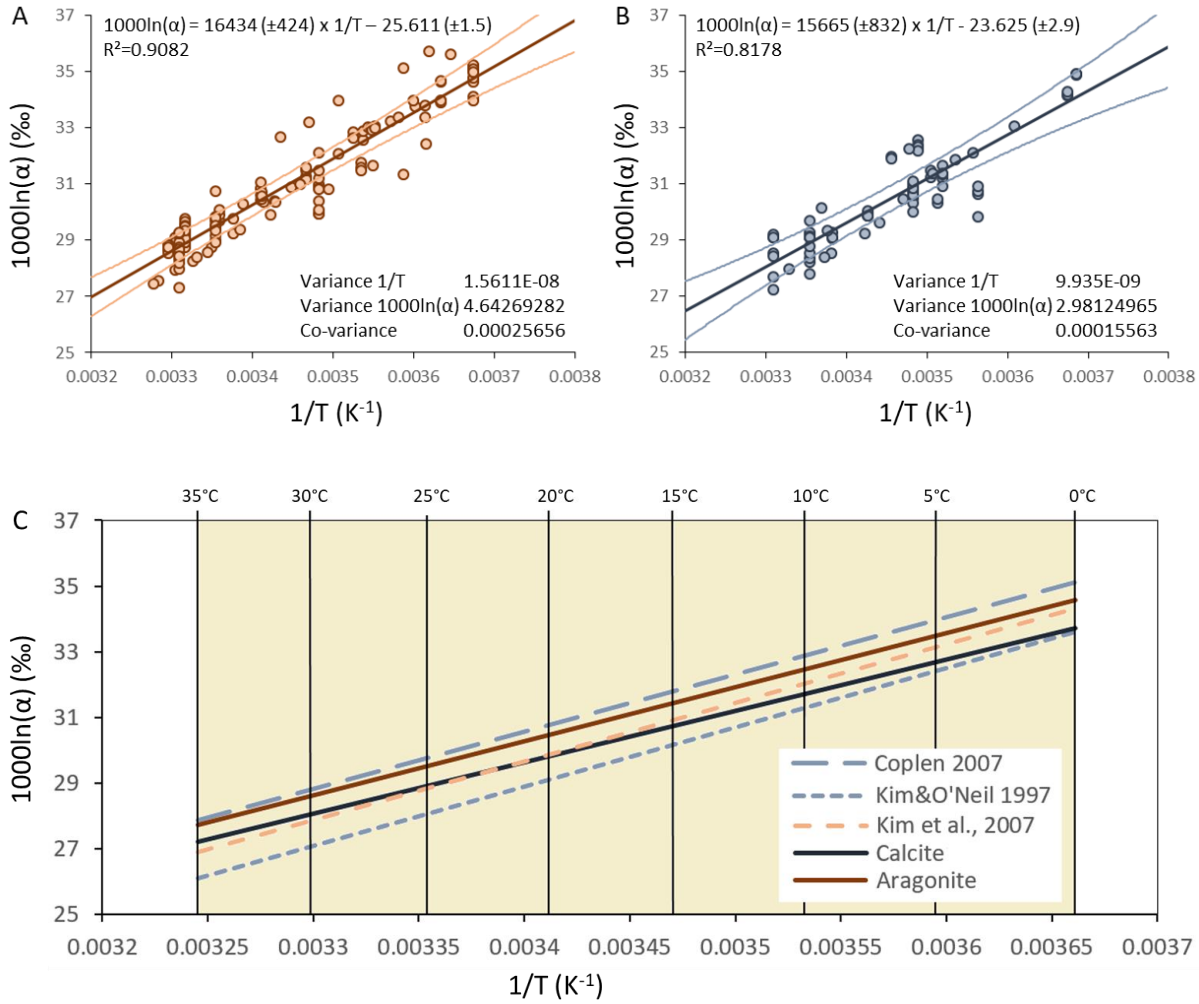

Fig. 3. Temperature dependence of the oxygen isotope fractionation between water and calcite and aragonite, respectively.

Compilation of empirical oxygen isotope fractionation data for aragonitic (A; in red; n = 139) and calcitic (B; in blue; n = 82) molluscs from various studies (Grossmann and Ku, 1986; Lecuyer et al., 2004; Lecuyer et al., 2012; Henkes et al., 2013; Caldarescu et al., 2021; de Winter et al., 2022; Huyghe et al., 2022; this study). Growth temperatures reflect measured water temperatures. For linear regressions (thick lines) in A and B, uncertainties in growth temperatures and 1000lnα were not considered as these were not consistently reported in each of these studies. Thin lines in A and B represent 95% confidence intervals of regression lines. A comparison of corresponding empirical regression lines with inorganic relationships obtained

by Coplen (2007) and Kim & O'Neil (1997) for calcite, and Kim et al. (2007) for aragonite is shown in C.

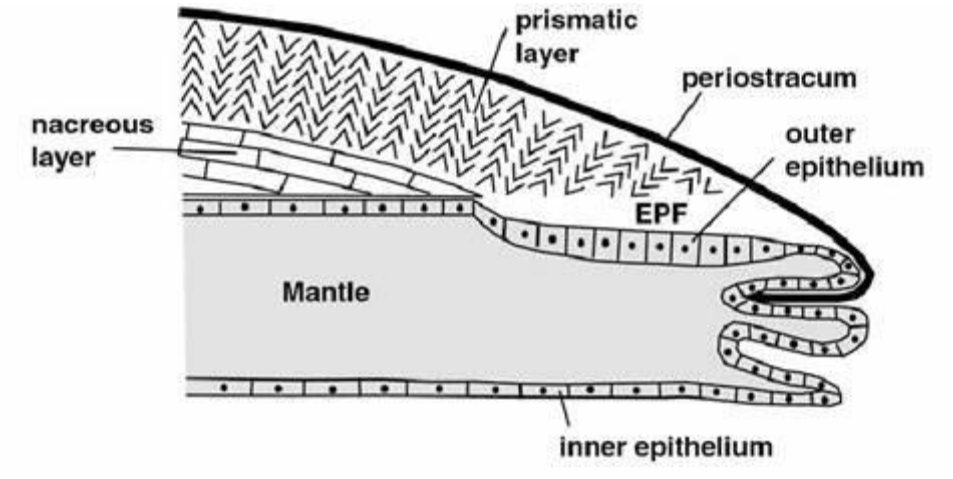

Fig. 4. Schematic drawing of the EPF (taken from Carré et al., 2006).

Shell formation in molluscs is orchestrated within the extrapallial fluid (EPF) which is enclosed by the outer epithelium (outermost cell layer of the mantle) and the periostracum (organic layer that covers the shell).

1084 **Table 1.** Metadata about investigated molluscs.

Sample	Species	Origin	Sampled part	Mineralogy
RG1	*Buccinum undatum* LINNAEUS 1758	Fife, Scotland, UK	Whole shell	Ar
RG2	*Patella vulgata* LINNAEUS 1758	Fife, Scotland, UK	Whole shell	Cc (>80%) Ar
RG2_U	*Patella vulgata* LINNAEUS 1758	Fife, Scotland, UK	Subsample RG2, no oxidative cleaning	Cc (>80%) Ar
RM1	*Modiolus modiolus* (LINNAEUS 1758)	Fife, Scotland, UK	Whole shell	Ar
RM2	*Spisula solida* (LINNAEUS 1758)	Fife, Scotland, UK	Whole shell	Ar
AI_006	*Arctica islandica* (LINNAEUS 1767)	Grown in culture (NIOZ), NL	Bulk sample	Ar
CHA_M_050	*Arctica islandica* (LINNAEUS 1767)	Dredged from NE coast of Iceland	Bulk sample (dual clumped data in Staudigel et al., 2023)	Ar
CHA_M_062	*Arctica islandica* (LINNAEUS 1767)	Dredged from NE coast of Iceland	Bulk sample (dual clumped data in Staudigel et al., 2023)	Ar
M2-Sf	*Magallana gigas* (THUNBERG 1793)	Mokbaai, Texel, NL	Seasonally averaged, entire hinge, foliated microstructure Geochemical data in de Winter et al., 2021	Cc
M2Sv	*Magallana gigas* (THUNBERG 1793)	Mokbaai, Texel, NL	Seasonally averaged, 2nd growth year Geochemical data in de Winter et al., 2021	Cc
ME_002	*Mytilus edulis* LINNAEUS 1758	Grown in culture (NIOZ), Grevelingen, NL	Bulk sample, Respiration rate data in Jansen et al., 2007	Cc+Ar
ME_003	*Mytilus edulis* LINNAEUS 1758	Grown in culture (NIOZ), Grevelingen, NL	Bulk sample, Respiration rate data in Jansen et al., 2007	Cc+Ar
Shell UC	*Hippopus porcellanus* ROSEWATER 1982	Antique trade	Along growth lines (Nooitgedacht et al., 2021)	Ar
Shell UH	*Hippopus porcellanus* ROSEWATER 1982	Antique trade	Along growth lines (Nooitgedacht et al., 2021)	Ar
TS2	*Tridacna Squamosa* LAMARCK 1819	Aquarium, Royal Burgers' Zoo, Amden, NL	Part of the inner shell	Ar
WS2	*Hiatella arctica* (LINNAEUS 1767)	White Sea, RU	Avoiding areas of muscle attachment and hinge	Ar
WS3	*Tridonta borealis* (*Astarte borealis*) (SCHUMACHER 1817)	White Sea, RU	Avoiding areas of muscle attachment and hinge	Ar
FG1	*Sycostoma* sp. COX 1931	Barton on Sea, England, UK	Whole shell	Ar
FG2	*Turricula (Orthosurcula) rostrata* (SOLANDER 1766)	Barton on Sea, England, UK	Whole shell	Ar
FG3	*Strombus athleta* (SOLANDER 1766)	Barton at Sea, England, UK	Whole shell	Ar

FM1	*Bathytormus sulcata* (SOLANDER 1766)	Barton at Sea, England, UK	Whole shell	Ar
FM2	*Arcturellina pusilla* (DESHAYES 1858)	Barton at Sea, England, UK	Whole shell	Ar

*NOIZ: Koninklijk Nederlands Instituut voor Onderzoek der Zee

Table 2. Stable and clumped isotope data of investigated molluscs. n represents number of analysed replicates.

Sample	**$\delta^{18}O_{CO2}$ VSMOW [‰]**	**$\delta^{18}O_{CO2}$ VPDB [‰]**	**$\delta^{18}O_{CC}$ VSMOW [‰]**	**$\delta^{18}O_{CC}$ VPDB [‰]**	**$\delta^{13}C$ VPDB [‰]**	**Δ_{47} [‰]**	**Δ_{47} 95% CI [‰]**	**Δ_{48} [‰]**	**Δ_{48} 95% CI [‰]**	**n**
RG1	41.31	10.08	32.50	1.53	1.12	0.649	0.006	0.255	0.019	9
RG2	40.99	9.77	32.60	1.63	0.93	0.642	0.004	0.288	0.013	21
RG2*	40.93	9.71	32.48	1.51	0.90	0.644	0.005	0.290	0.015	15
RG2_U	41.13	9.91	32.68	1.71	1.01	0.638	0.007	0.283	0.023	6
RM1	41.12	9.90	32.30	1.34	1.49	0.645	0.006	0.254	0.019	9
RM2	41.03	9.81	32.21	1.25	0.77	0.645	0.006	0.250	0.020	8
AI_006	41.79	10.55	32.97	1.99	0.05	0.632	0.007	0.271	0.021	7
CHA_M_050	42.76	11.49	33.96	2.95	1.29	0.647	0.007	0.262	0.021	7
CHA_M_062	43.19	11.90	34.36	3.34	2.30	0.655	0.007	0.264	0.021	7
M2-Sf	37.58	6.46	29.21	-1.66	-2.00	0.612	0.006	0.263	0.019	7
M2-Sv	37.72	6.60	29.35	-1.52	-1.84	0.632	0.006	0.266	0.018	8
ME_002	39.26	8.09	30.88	-0.04	-1.70	0.621	0.006	0.253	0.020	8
ME_003	39.19	8.02	30.81	-0.11	-1.41	0.622	0.007	0.260	0.021	7
Shell UC	37.99	6.86	29.20	-1.67	2.91	0.591	0.006	0.242	0.020	8
Shell UH	37.72	6.60	28.93	-1.93	2.44	0.586	0.006	0.239	0.019	9
TS2	36.69	5.60	27.91	-2.92	-7.42	0.597	0.006	0.240	0.020	8
WS2	41.21	9.98	32.39	1.43	1.64	0.667	0.006	0.259	0.018	10
WS3	37.30	6.19	28.52	-2.33	-0.05	0.645	0.006	0.286	0.019	9
Fossil Samples										
FG1	36.61	5.52	27.83	-3.00	0.08	0.617	0.006	0.242	0.019	9
FG2	36.96	5.86	28.18	-2.66	-2.08	0.608	0.006	0.256	0.019	9
FG3	36.65	5.56	27.87	-2.96	-1.88	0.608	0.006	0.239	0.019	9
FM1	37.14	6.04	28.36	-2.48	1.20	0.607	0.006	0.249	0.019	9
FM2	35.73	4.67	26.96	-3.84	0.58	0.600	0.006	0.243	0.019	9

Table 3. Independently constrained growth temperatures, Δ_{47}-derived growth temperatures and independently constrained $\delta^{18}O_{SW}$.

Sample	**Growth temperature**	**Δ_{47} derived T (°C)**	**T-range 95% CI (°C)**	**$\delta^{18}O_{SW}$ (‰ vs VSMOW)**
RG1	MASST 9.7°C, Seasonal range 6-14°C	6.9	4.7-9.0	0.2 (Harwood et al., 2008)
RG2	MASST 9.7°C	9.1	7.5-10.7	0.2 (Harwood et al., 2008)
RM1	MASST 9.7°C	8.2	6.0-10.5	0.2 (Harwood et al., 2008)
RM2	MASST 9.7°C	8.2	5.9-10.5	0.2 (Harwood et al., 2008)
AL_006	Cultured at 12°C	12.3	10.0-14.6	-1.55
CHA_M_050	Water T at time of collection 3-4°C (Pederson et al., 2019); Up to 10°C in summer	7.6	5.4-9.9	Rough estimate ~0 (Schmidt et al., 1999)
CHA_M_062	Water T at time of collection 3-4°C (Pederson et al., 2019); Up to 10°C in summer	5.1	2.9-7.4	Rough estimate ~0 (Schmidt et al., 1999)
M2-Sf	MASST 11.5°C Seasonal range 4.5-19.2°C	19.0	16.9-21.1	-1.55
M2-Sv	MASST 11.5°C Seasonal range 4.5-19.2°C	12.1	10.2-14.0	-1.55
ME_002	Mean growth temperature 16.2°C Seasonal range 5-25°C	16.1	13.9-18.3	-1.55
ME_003	Mean growth temperature 16.2°C Seasonal range 5-25°C	15.4	13.1-17.7	-1.55
Shell UC	est. 27-31°C (based on geographic occurrence)	26.3	24.0-28.7	~0.1 (Schmidt et al., 1999)
Shell UH	est. 27-31°C (based on geographic occurrence)	28.3	26.1-30.5	~0.1 (Schmidt et al., 1999)
TS2	25.9°C, up to 26.8°C in summer	24.4	22.2-26.6	-1.05 (measured)
WS2	MASST 5.56°C (range of -1.7- >10°C possible)	1.4	-0.4-3.2	-3.24
WS3	MASST 5.56°C (range of -1.7- >10°C possible)	8.3	6.4-10.3	-3.24

Table 4. Δ_{47}-derived temperatures and reconstructed seawater $\delta^{18}O$ for Eocene samples.

Sample	Δ_{47} **derived T (°C)**	**T-range 95% CI (°C)**	**Reconstructed $\delta^{18}O_{sw}$ (‰ vs VSMOW)**	**$\delta^{18}O_{SW}$-range 95% CI (‰ vs VSMOW)**
FG1	17.3	15.1-19.6	-3.5	-3.1 - -3.9
FG2	20.5	18.3-22.8	-2.6	-2.1 - -3.0
FG3	20.3	18.1-22.6	-2.9	-2.5 - -3.3
FM1	20.7	18.4-23.1	-2.3	-1.9 - -2.8
FM2	23.2	21.0-25.6	-3.2	-2.8 - -3.6